15-12-2012

Fibroblast growth factor homologous factor 1 interacts with NEMO to regulate NF-κB signaling in neurons.

Hans-Georg König
Royal College of Surgeons in Ireland

Beau J. Fenner
Royal College of Surgeons in Ireland

Jennifer C. Byrne
Royal College of Surgeons in Ireland

Robert F. Schwamborn
Royal College of Surgeons in Ireland

Tytus Bernas
Royal College of Surgeons in Ireland

See next page for additional authors

Citation

Konig HG, Fenner BJ, Byrne JC, Schwamborn RF, Bernas T, Jefferies CA, Prehn JHM. Fibroblast growth factor homologous factor 1 interacts with NEMO to regulate NF-κB signaling in neurons. Journal of Cell Science. 2012;125(24):6058-70.

Authors
Hans-Georg König, Beau J. Fenner, Jennifer C. Byrne, Robert F. Schwamborn, Tytus Bernas, Caroline A. Jefferies, and Jochen HM Prehn

Fibroblast growth factor homologous factor 1 interacts with NEMO to regulate NF-κB signaling in neurons

Hans-Georg König[1], Beau J. Fenner[1,2,a], Jennifer C. Byrne[3], Robert F. Schwamborn[1,b], Tytus Bernas[1,c], Caroline A. Jefferies[3] & Jochen H. M. Prehn[1,2]*

[1]Centre for the Study of Neurological Disorders (CSND), Department of Physiology & Medical Physics, [2]Centre for Systems Medicine (CSM), Department of Physiology & Medical Physics, [3]Molecular and Cellular Therapeutics, Royal College of Surgeons in Ireland, 123 Saint Stephen's Green, Dublin 2, Ireland

[a]current address: Duke-NUS Graduate Medical School, 8 College Road, Singapore 169857, Singapore; [b]current address: University College Dublin, School of Biomedical and Biomolecular Science, Conway Institute, Dublin 4, Ireland; [c]current address: Laboratory of Functional and Structural Tissue Imaging, Nencki Institute of Experimental Biology, ul. Ludwika Pasteura 302-093 Warszawa, Poland

*Correspondence should be addressed to Prof. Jochen H. M. Prehn, Department of Physiology and Medical Physics, Royal College of Surgeons in Ireland, 123 Saint Stephen's Green, Dublin 2, Ireland. Tel.: +353-1-402-2255; Fax: +353-1-402-2447; E-mail: prehn@rcsi.ie

Running Title: FHF1 and neuronal NF-κB

Keywords: NF-kappa B / Fgf12 protein / I-kappa B Kinase / neuronal plasticity / protein interaction

Summary

Neuronal survival and plasticity critically depend on constitutive activity of the transcription factor nuclear factor-κB (NF-κB). We here describe a role for a small intracellular fibroblast growth factor homologue, the fibroblast growth factor homologous factor 1 (FHF1/FGF12) in the regulation of NF-κB activity in mature neurons. FHF's have previously been described to control neuronal excitability, and mutations in FHF isoforms give rise to a form of progressive spinocerebellar ataxia. Using a protein-array approach, we identified FHF1b as a novel interactor of the canonical NF−κB modulator IKKγ/NEMO. Co-immunoprecipitation, pull-down and GAL4-reporter experiments, as well as proximity ligation assays confirmed the interaction of FHF1 and NEMO, and demonstrated that a major site of interaction occurred within the axon initial segment. *Fhf1* gene silencing strongly activated neuronal NF-κB activity and increased neurite lengths, branching patterns and spine counts in mature cortical neurons. The effects of FHF1 on neuronal NF-κB activity and morphology required the presence of NEMO. Our results imply that FHF1 negatively regulates the constitutive NF-κB activity in neurons.

Introduction

In the nervous system, the transcription factor NF-κB consists of hetero- or homodimers made up of p50, p65 or c-Rel (Schmidt-Ullrich et al., 1996; Kaltschmidt and Kaltschmidt, 2009). The N-terminal Rel homology domain (RHD) contains sequences responsible for dimerization, nuclear translocation and DNA-binding. In contrast to p50, p65/RelA and c-Rel contain a strong transactivation domain. In the so-called canonical pathway, NF-κB complexes are retained in the cytoplasm by sequestration to the ankyrin-repeat domains of the nuclear factor κB inhibitor-α (IκBα), while signal-induced N-terminal phosphorylation results in proteasomal degradation of the latter and translocation of the transcription factor to the nucleus (Perkins, 2006). The IKK-complex, a heteromeric holoenzyme that phosphorylates IκBα on two highly conserved serine residues (Ser32, Ser36), is composed of three specific subunits IKKα, IKKβ, and a varying number of the scaffold protein IKKγ, also known as NEMO (NF-κB essential modulator; Yamaoka et al., 1998). NEMO is considered to be a key regulator of NF-κB signaling, as genetic ablation results in diminished activation of NF-κB in response to a number of inflammatory stimuli (Rothwarf et al., 1998; Makris et al., 2002; van Loo et al., 2006).

NF-κB controls neurite outgrowth in the developing CNS and PNS (Gutierrez et al., 2005; Li et al., 2010), and is thought to be involved in the regulation of learning and memory (Albensi and Mattson, 2000; Meffert et al., 2003). Additionally, calcium influx induced by synaptic transmission is considered to be the driving force for constitutive neuronal NF-κB activity in the adult nervous system (Lilienbaum and Israel, 2003; Meffert et al., 2003; O'Sullivan et al., 2010). In contrast, little is known regarding neuron-specific proteins in control of NF-κB signaling. Considering the important role of NEMO in the canonical NF-κB signaling pathway, we considered NEMO a valid bait to identify new upstream regulators of neuronal NF-κB signaling. Using a protein microarray approach, we identified the intracellular protein, fibroblast growth factor homologous factor 1b (FHF1b) as a novel interactor of NEMO, and investigated the biological role of FHF1b in the regulation of neuronal NF-κB signaling, and in the maintenance of neuronal morphology in adult neurons.

Results

Protein microarrays identify FHF1b as a novel interaction partner of NEMO.

Affinity-purified and biotinylated full-length human NEMO was used to probe a human protein microarray containing approximately 8,200 full-length proteins to identify novel factors controlling NF-κB signaling (Fenner et al., 2010; Fig. 1A). Two canonical NEMO interactors, IKKα and IKKβ, were among the top hits based on Z score analysis, demonstrating the validity and robustness of this approach (Fig. 1B). Intriguingly, a new neuron-specific binding partner, fibroblast growth factor homologous factor 1b (FHF1b/FGF12b), was among the highest affinity hits (Fig. 1A, B and Suppl. Fig. 1). Initial experiments confirmed positive interaction between overexpressed FHF1b and NEMO in HEK293 cells, as determined by co-immunoprecipitation (Fig. 1C) and GST pulldown assays (Fig. 1D). Additionally, mammalian two-hybrid assays in neuronal PC12 cells and primary neurons (Figs. 1E and F) demonstrated that co-expression of GAL4-binding domain tagged NEMO and transactivation domain tagged FHF1b significantly enhanced GAL4-driven normalized luciferase activity (Fig. 1F, control 0.04 ± 0.02, MyoD/Id 0.47 ± 0.18, NEMO/FHF1b 2.70 ± 1.40).

Endogenous FHF1 protein is expressed at the axon initial segment of mature hippocampal neurons in culture and in the adult mouse cortex.

Previous studies using green fluorescent protein (GFP)-tagged FHF1a/b indicated that these proteins localize to the axon initial segment (AIS; Goldfarb et al., 2007; Wang et al., 2011). The AIS is characterized by a high accumulation of the cytoskeletal scaffolding protein ankyrinG, which is involved in the attachment of further AIS-specific protein complexes (Rasband, 2010). We found that cultured neurons expressed *Fhf1* mRNA (Suppl. Fig. 2E) and displayed a marked FHF1 immunofluorescence in the AIS of mature neurons (Fig. 2A). Specificity of the FHF1 antibody was confirmed by plasmid-mediated overexpression of FHF1 and *Fhf1*-RNA interference in cultured cortical neurons (Fig. 2B,C and Suppl. Fig. 3A). We also found endogenous FHF1-immunoreactivity in extracts obtained from the neocortex of adult mice (Fig. 2D). Furthermore, we used a pepsin-based antigen-retrieval method on floating sections (Lorincz and Nusser, 2008), obtained from the cortex of adult mice, to detect endogenous FHF1-immunoreactivity *in situ* at the AIS (Fig. 2E, and F as negative control). We observed that this was closely associated with the ankyrinG-positive AIS (Fig. 2G).

FHF1 interacts with NEMO and the IKK-complex at the AIS *in situ*.

Having established the expression of FHF1 in the AIS, we next examined whether FHF1 interacted with NEMO and the IKK signaling complex at this site. Detergent extraction of living neurons

isolates cytoskeleton-associated structures, while cytosolic proteins are eliminated prior to immunofluorescence analyses (Winckler et al., 1999). FHF1 immunoreactivity clearly decorated the axon-initial segment in mature cortical neurons following detergent extraction of somatic proteins prior to fixation in vitro (Fig. 3A, Suppl. Fig. 3B). We then investigated whether NEMO was localized in the AIS. Similar to FHF1, NEMO immunoreactivity decorated the AIS in mature cortical neurons following detergent-extraction (Fig. 3B, Suppl. Fig. 3C). Depletion of *Nemo* mRNA using siRNA in mature cortical neurons significantly reduced NEMO immunoreactivity and phosphorylated-IKKα/β immunoreactivity in the AIS (Fig. 3C,C', decrease of 45.3 % ± 8.01 %; and Suppl. Fig. 2A-D, specificity of the phospho-IKKα/β antibody was examined in Suppl. Fig. 3D). Studies in cortical neurons using confocal microscopy revealed FHF1 immunoreactivity in speckled clusters along the phospho-IKKα/β-positive AIS (Fig. 3D,E). Quantitative co-localization analyses confirmed that the highest immunofluorescence intensities of FHF1 and pIKKα/β occurred within the cell membrane along the AIS (Fig. 3D,E; Pearson's correlation coefficient Rr = 0.74 (AIS only, D) and Rr = 0.52 (non-AIS, D); Rr = 0.68 (E, AIS)). Subcellular fractionation of adult brain extracts~~, furthermore~~ revealed a high expression of FHF1 protein in the cytosolic and lipid fractions, while NEMO concentrated in the nuclei, mitochondria and likewise in the lipid fraction (Fig. 3F).

To show interaction of FHF1 with the proteins of the IKK-complex *in situ*, we employed proximity ligation assays (PLA). These assays combine antibody-labelling with signal detection by rolling-circle amplification of secondary antibody-linked oligonucleotides and subsequent fluorescent staining, thus indicating protein interactions by detection of molecular proximity *in situ,* similar in sensitivity to fluorescence resonance energy transfer (Soderberg et al., 2006; Fig. 4A). Firstly, we overexpressed NEMO and FHF1b together with EGFP in primary cortical neurons. Transfected cells displayed a punctate PLA fluorescence across the neuronal cell body, and enrichment in the proximal area of some neurites (Figs. 4B,C). We also detected a marked accumulation of PLA-spots within the AIS in cells transfected with either, FHF1b (Fig. 4D) or NEMO (Fig. 4E) alone and probed for NEMO-FHF1b interactions (Fig. 4D,E). Cells were additionally immunostained for ankyrinG to confirm the localization of PLA-spots to the AIS (Fig. 4E). As a negative control, we performed PLA assays with EB1 (Piehl and Cassimeris, 2003), a microtubule-associated protein that is significantly enriched in the AIS (Nakata and Hirokawa, 2003). PLA assays using EB1-GFP did not reveal a significant association with the IKK-complex (Fig. 4F). Quantification of PLA spots showed that FHF1-NEMO interactions were significantly more frequently observed in the AIS than interactions in the negative control experiment (Fig. 4G, 28 ± 4 vs. 3 ± 1 spots). Next, we examined interactions between endogenous NEMO and FHF1 proteins by PLA assay. We detected PLA fluorescent aggregates – suggesting NEMO and FHF1 interactions - in the neuronal soma and

proximal neurites of non-transfected cells, resembling the localization of the AIS (Fig. 4H), but no apparent fluorescence was found in the nuclei. Similar results were obtained using FHF1 and IKKβ primary antibodies, suggesting binding of FHF1 to the IKK complex in the AIS and soma (Fig. 4I). Additional post-PLA ankyrinG-labelling and confocal microscopy confirmed the interaction of endogenous FHF1 and NEMO occurred along the ankyrinG-positive AIS membrane (Fig. 4J). Furthermore, endogenous FHF1-NEMO molecular proximity was observed more frequently in the AIS, as in post-synaptic densities (PSD-95), MAP-2 positive dendrites, or as compared to the AIS of the negative control reaction (Fig. 4K and Suppl. Fig. 4). Proximity-ligation between overexpressed NEMO and overexpressed IKKβ protein served as a positive control, while no proximity-ligation was observed using FLAG and XPress antibodies (Fig. 4L,M).

The interaction between FHF1 and NEMO limits NEMO's wild-type-, K48- and K63-linked polyubiquitination and IKK-kinase activity.

K63-linked polyubiqitination of NEMO has been identified as essential for IKK-signalsome activity via recruitment of upstream activators TAB2/TAB3 to the signalsome and thus facilitates the activation of the IKKβ-Kinase TAK1 (Gautheron and Courtois, 2010; reviewed in Schmukle and Walczak, 2012). To assess the effects of FHF1 on NEMO and IKK signalsome activity, we determined the phosphorylation status of the inhibitor of κB (IκBα) following a canonical NF-κB stimulus (lipopolysaccharide). Intriguingly, we found that FHF1b-transfection induced an ablation of LPS-induced phosphorylation of the IκBα protein and thus might be seen as a suppressor of the activity of the NF-κB transcription factor (Fig. 5A). Having demonstrated that FHF1b over-expression resulted in reduced IKK-signalsome activity, we next determined whether FHF1b affected polyubiquitination of NEMO. Co-transfection of FHF1b reduced the basal level of ubiquitination of NEMO (Fig. 5B), indicating that FHF1 negatively regulated polyubiquitination of NEMO. To determine if FHF1b was affecting either K48-linked (thus implicating FHF1b in the regulation of NEMO stability) or K63-linked polyubiquitination (and hence assembly of the IKK-signalsome), we employed ubiquitin-mutant proteins in this assay, where all five lysine-residues are mutated to arginine, except residues K48 or K63 (R48K, R63K, Ramakrishna et al., 2011), respectively. Interestingly, FHF1b co-transfection resulted in reduced R48K and R63K polyubiquitinated NEMO, indicating that, in addition to regulating NEMO activity, FHF1 may also affect NEMO stability (Fig. 5C). This finding is supported by analysis of NEMO protein levels following overexpression of FHF1b in primary neurons, in which enhanced NEMO levels were observed, with no alteration to p65/NF-κB levels (Fig. 5D).

Constitutive transcriptional activation by NF-κB is repressed by FHF1b overexpression and potentiated by FHF1 silencing.

Having demonstrated that FHF1 reduced IKK-signalsome activity and K63-linked polyubiquitination of NEMO, we next examined the impact of FHF1 on NF-κB activation. First, endogenous constitutive NF-κB activity during development was probed using antibodies specific to active p65/NF-κB. Nuclear localization of the activated transcription factor peaked around DIV7 and subsided thereafter (Suppl. Fig. 5A). FHF1 expression levels during in vitro development were obtained by immunofluorescence analyses in dissociated cortical neurons to determine optimized time points for functionally meaningful gene silencing experiments. FHF1 expression levels increased consistently during in vitro development up to DIV18, when a strong co-localization to the ankyrinG-positive axon-initial segment and less somatic or nuclear accumulation was observed (Fig. 6A). We then employed NF-κB-specific reporter-gene assays to examine the influence of FHF1 on p65 transactivation potential. Interestingly, overexpression of FHF1b in primary mature neurons resulted in a reproducible and significant decrease in NF-κB-dependent transcriptional activation (Fig. 6B). Expression of two FHF1 splice variants, FHF1a and FHF1b (truncated N-terminus), in mammalian cells prevented selective gene silencing of FHF1b. Instead, we used small-hairpin RNA directed against a common region of both splice variants and obtained a significant reduction of total FHF1 mRNA in transfected neurons (Fig. 2C, Suppl. Fig. 1E). Most notably, NF-κB activity increased significantly by approximately three-fold compared to controls in FHF1-depleted mature neurons (DIV15-19, Fig. 6D,E), in keeping with the inhibitory effects of FHF1 on polyubiquitination of NEMO and phosphorylation of IκBα. No significant impact of *Fhf1* silencing on NF-κB activity was measured in early and immature cortical neurons, exhibiting relatively low FHF1 protein expression levels in culture (DIV4-7, Fig. 6A, ~~and~~ C). Sequence-intrinsic effects were additionally confirmed by transfection of single shRNA constructs into rat neurons. Single *Fhf1*-mRNA silencing constructs induced κB-dependent luciferase activity less effectively than co-transfection with two silencing vectors (Suppl. Fig. 5B). As expected by sequence disparities, the constructs failed however to induce κB-dependent luciferase activity in a human cell line (Suppl. Fig. 5C), thus excluding unspecific effects.

We next sought to determine the requirement for NEMO in the repressive effect of FHF1 on NF-κB transcriptional activity. Ablation of FHF1 and NEMO in cortical neurons resulted in reductions of the respective mRNA copy numbers (Figs. 6G,H). Co-silencing of NEMO and FHF1 in cortical neurons demonstrated that the suppressive effect of FHF1 on NF-κB activity indeed required NEMO (Fig. 6E, *Fhf1* shRNA increase by 3.30 ± 1.14 fold; *Nemo* and *Fhf1* shRNA decrease by 0.55 ± 0.44 fold over control). Additionally, transfecting increasing amounts of NEMO effectively

neutralized the suppressive effect of FHF1b on NF-κB activity, while a NEMO mutant defective in ubiquitin-binding failed to enable NF-κB activity, establishing FHF1b upstream of NEMO-induced signal transduction (Fig. 6F; FHF1b-induced decrease by 0.25 ± 0.10 fold, FHF1b and NEMO wt (2.5 µg) increase by 2.48 fold ± 0.07, FHF1b and NEMO-L329P (2.5 µg) decrease by 3.99 ± 0.32 fold).

FHF1 modulates NF-κB-dependent control of structural homeostasis.

Activation of NF-κB has been implicated in neurite outgrowth (Gutierrez et al., 2005). We next sought to determine whether FHF1 controls the neuronal morphology of mature cortical neurons with established neurite trees. Firstly, we derived Sholl profiles by manual evaluation of p65-depleted neurons to examine the implication of the transcription factor in the maintenance of neuronal morphology. Ablation of p65 in mature neurons significantly reduced neuronal arborisation and neurite length compared to control neurons (Fig. 7A,A'). We next investigated whether silencing of FHF1 expression resulted in the opposite effect. Interestingly, FHF1 ablation increased the number of intersections across the neurite tree (Fig. 7B,B'). These findings were further supported with a high-content imaging approach on mature cortical neurons (Buchser et al., 2010), which revealed a significant increase in relative neurite length and branching point counts in FHF1-depleted neurons (increase of 39.5 ± 9.9 % and increase of 42.1 ± 11.6), while p65 ablation resulted in the opposite (Fig. 7C-E, decrease of 19.9 ± 4.5 % and 13.6 ± 6.6 %, DIV15 - 20). In accordance with the above, Sholl profiles obtained from NEMO-depleted neurons revealed a significant reduction of neurite lengths and branching patterns in mature neurons (Fig. 7F,G), with a comparable result using the high-content imaging approach (Fig. 7G'). We also investigated whether the increase in neurite growth induced by FHF1 depletion required NEMO by comparing the effects of *NEMO*, *Fhf1*, and combined *NEMO* and *Fhf1* gene silencing over a period of five days. An increase in average neurite length, neurite counts and a trend towards increased branching was observed in FHF1-depleted neurons, while a decrease was noted in NEMO-depleted cells. As shown by double-silencing of FHF1 and NEMO, the effect on NF-κB achieved by co-silencing of NEMO was dominant over FHF1 ablation, suggesting that the regulation of neuronal morphology by FHF1 required NEMO (Figs. 7H-J).

FHF1 regulates neurite spine densities.

Finally, we sought to determine whether FHF1 also modulates spine structural plasticity. Cortical neurons at stage 5 (DIV15-25) in culture exhibit elaborate spine patterns on their dendrites (Dotti et al., 1988; Barnes and Polleux, 2009). We determined the impact of FHF1 depletion on their spine patterns using shRNA-mediated mRNA silencing. Neuronal spines were detected using a voxel-

clustering algorithm based on the skeletonization of 3D-stacks (Rodriguez et al., 2006; Rodriguez et al., 2008). Concurrent with our morphological findings, the FHF1-depleted neurons exhibited an increase in average neurite length per unit volume (Fig. 8A,B, *Scr* shRNA 712.25 ± 64.97 % to *Fhf1* shRNA 1015.42 ± 181.7 %). Likewise, image analysis revealed a significant increase in the average spine count per unit volume (Fig. 8C,D, 303.0 ± 66.9 % to 719.4 ± 142.7 %) and in average spine density per neurite shaft length (Fig. 8C,E, 39.9 ± 5.9 to 70.1 ± 5.1 spines per 100 µm neurite shaft).

Discussion

In the present study, we identified an AIS-enriched protein, the fibroblast growth factor homologous factor 1 (FHF1/FGF12), as a novel interactor of the canonical NF–κB modulator IKKγ/NEMO within mature neurons. We furthermore demonstrate that a disruption of this interaction impacts on NF-κB signalling and maintenance of neuronal morphology. It is well established that cortical neurons exhibit a pronounced constitutive activity of the transcription factor NF-κB (Kaltschmidt et al., 1994) and its trans-activating capacity is considered essential for development and adult neuronal tissue maintenance (Schmidt-Ullrich et al., 1996; Bhakar et al., 2002; Chiarugi, 2002; Fridmacher et al., 2003). The continuous drive for the activation of NF-κB was suggested to be imparted by either post-synaptic activation mediated through the neurotransmitter glutamate or spontaneous calcium fluctuations (Kaltschmidt et al., 1995; Lilienbaum and Israel, 2003). This is mediated via post-synaptic activation and retrograde transport of p65/NF-κB from dendrites to the nucleus, using dynein-mediated transport mechanisms (Meffert et al., 2003; Mikenberg et al., 2007). We here demonstrate the potential existence of a second source of constitutive NF-κB activity in neurons that is controlled by FHF1 and requires NEMO, in line with the presumed essential role of NEMO in activation of the IKK-complex by a range of established stimuli (Yamaoka et al., 1998; Solt et al., 2009; Fenner et al., 2010).

Using an unbiased protein microarray approach, we identified protein interactions between NEMO and FHF1b, a family member of fibroblast growth factor homologous factors (FHF), which have repeatedly been described to be highly concentrated at the AIS in earlier studies (Lou et al., 2005; Goldfarb et al., 2007; Goetz et al., 2009; Laezza et al., 2009). FHF's are a subfamily of the fibroblast growth factor (FGF) superfamily, expressed throughout the developing nervous system (Smallwood et al., 1996). However these factors lack N-terminal secretion sequences (Goldfarb, 2005) and are considered *bona fide* intracellular proteins without the capability to bind to FGF-receptor complexes (Olsen et al., 2003; Goldfarb, 2005). FHFs share considerable mutual protein sequence homology (Goldfarb, 2005). Mutations in FHF4 cause ataxia (Wang et al., 2002), dystonia and dyskinesia in mice and the autosomal dominant missense mutation $FHF4^{F145S}$ gives rise to a form of progressive spinocerebellar ataxia (SCA27; van Swieten et al., 2003; Xiao et al., 2007). Complete genetic ablation of FGF14 affects synaptic transmission and likewise results in ataxia and paroxysmal dyskinesia (Wang et al., 2002; Laezza et al., 2007; Xiao et al., 2007), with the phenotype of FHF1/FHF4 double-knockout animals being more pronounced (Goldfarb et al., 2007).

Even though FHF1 expression in the AIS, similar to its relatives FHF2-4, has been reported for over-expressed FHF1 fusion proteins (Goldfarb et al., 2007; Wang et al., 2011), its endogenous accumulation at the AIS *in situ* had not yet been documented. We found that upon antigen

unmasking, FHF1 antibodies decorated the AIS in the neocortex and hippocampus, regions with considerably high constitutive NF-κB activity (Bhakar et al., 2002; Kaltschmidt et al., 1994; O'Sullivan et al., 2010). This pattern is also in line with FHF-transcript expression in the developing nervous system (Smallwood et al., 1996). We also demonstrated a clustering of the IKK-complex (i.e activation-loop phosphorylated IκB-kinase and NEMO), and an interaction of FHF1 and NEMO in the AIS. In this context, it is interesting to note that other studies recently reported a clustering of constitutively-phosphorylated proteins of the NF–κB signal transduction cascade in the AIS (activation-loop phosphorylated IKKα/β, Ser32, 36-phosphorylated IκBα and transactivation-domain Ser536-phosphorylated NF-κB/p65; Schultz et al., 2006; Sanchez-Ponce et al., 2008). We found that silencing of FHF1 protein levels resulted in a prominent, three to four-fold up-regulation of κB-dependent reporter-gene transactivation, whereas overexpression of FHF1 resulted in a suppression of NF-κB, which could be alleviated by increasing levels of NEMO. Normally a membrane-receptor associated scaffolding protein (Windheim et al., 2008), nuclear NEMO is exported to the cytosol in resonse to genotoxic stimuli and calcium-signaling (Berchtold et al., 2007). NEMO has also been shown to link the IKK-complex to the actin cytoskeleton and transport via Myo1c (Nakamori et al., 2006). NEMO binds to K63-linked polyubiqitinated upstream complexes, a process which is thought to facilitate IKK-complex formation and phosphorylation (Schmukle and Walczak, 2012). We observed elevated NEMO levels in neurons following FHF1b expression, possibly the consequence of decreased proteasomal turnover due to decreased K48-linked polyubiquitination. Likewise, we observed a decrease in K63-linked polyubiquitinated NEMO. As this process is believed to favour NEMO-dependent signal transduction towards IKK, "activated NEMO" may decrease in the presence of FHF1b. As we found FHF1b itself was polyubiquitinated, it is reasonable to hypothesize that NEMO binds directly to the attached K63-linked chains on FHF1b. We hope that future work will elucidate the inderdependencies or cross-talk between the polyubiquitination patterns of the two proteins. In summary, our results suggest FHF1 interaction with NEMO may sequestrate the protein from the IKK-complex and limit NEMO's Lys 63-linked poly-ubiquitination (Tang et al., 2003; Henn et al., 2007) or nuclear translocation. We cannot fully exclude that FHF1 regulates neuronal NF-κB at sites other than the AIS, particularly the soma, nevertheless our data provide important evidence for a NEMO-dependent regulation of constitutive NF-κB signalling by FHF1. Notably, we found developmental regulation of constitutive activation of NF-κB peaked around DIV7 and decreased thereafter. Although we do not presume FHF1 to be the only regulator of constitutive NF-κB, this decline may partly be explained by the rise in FHF1 expression levels.

We also found a marked increase in the number of neurite branching points upon silencing of FHF1 in fully-differentiated neurons, along with a significant increase in neurite numbers and lengths. Our data suggest that this effect is mainly achieved through FHF1 interaction with NEMO. Consistently, the opposite effects were observed after NEMO or p65 silencing. Furthermore, the FHF1-silencing phenotype was regulated in a NEMO-dependent manner. NF-κB activation has previously been linked to enhanced neurite outgrowth (Gutierrez et al., 2005; Li et al., 2010). Recent evidence implicates NF-κB-dependent transcription of PKA and FOXO1 in axogenesis (Imielski et al., 2012), while pharmacologic interference with IKK activation has been shown to slow down axon outgrowth and AIS development (Sanchez-Ponce et al., 2008). We here show that constitutive NF-κB activity, mediated through a NEMO-dependent pathway, is necessary to maintain the morphology of established dendritic trees in differentiated neurons. Our results further suggest that the interaction of FHF1 with NEMO is required to maintain this state, and that any alteration in FHF1-NEMO interaction may lead to signficant changes in neuronal morphology and dendritic structural plasticity. In this context, it is interesting to note that disruption of the AIS cytoskeleton during ischemia has been suggested to contribute to neuronal injury, where proteolytic cleavage of ankyrinG is irreversible (Schafer et al., 2009). Loss of this important upstream anchor caused loss of neuronal polarity, a transition from axonal to dendritic identity and the formation of dendritic spines on the former axon (Hedstrom et al., 2008; Sobotzik et al., 2009). Additionally, recent evidence suggests that the cell-adhesion molecule Neurofascin186 is involved in the stabilization of the axon initial segment (Zonta et al., 2011). Finally, it has also been shown that the expression of a constitutively-active IKK increases spine density in neurons (Russo et al., 2009). We observed significantly enhanced dendritic spine counts on FHF1-ablated cells, suggesting that FHF1 is involved in spine plasticity (Segal, 2010). Our study therefore establishes FHF1 as an important regulator of structural plasticity and neuronal morphology.

Materials and Methods

Reagents and chemicals. Unless otherwise stated, chemicals were purchased from Sigma-Aldrich (Arklow, Ireland), Merck Chemicals (Nottingham, UK) or Tocris Bioscience (Bristol, UK). Cell culture media were purchased from Gibco-Invitrogen (Dun Laoghaire, Ireland). pre-designed HuSH-29 small-hairpin RNA-vector constructs from Origene, Rockville, MD, USA.

Cell culture. Primary cultures of cortical neurons were prepared from neonatal Sprague-Dawley rats as described previously described (König et al., 2005). Neurons were cultured in in NMEM-B27 media (1 x MEM, 1 mM sodium pyruvate, 26 mM $NaHCO_3$, 2 mM Glutamax®, 1 x B27 serum supplement and 33 mM β-D-Glucose (Sigma Aldrich) at 37°C in a humidified atmosphere containing 5 % (v/v) CO_2. Astrocyte content of cultures was kept to a minimum by treatment with 1 µM cytosine β-D-arabino-furanoside. Mature neurons in vitro were defined as stage 5 cultures (older than DIV15; Barnes and Polleux, 2009). Animal work was carried out under license from the Department of Health and Children of Ireland. Animal working procedures were additionally approved by the Research Ethics Committee of the Royal College of Surgeons in Ireland. Cell lines were grown according to standard techniques and transfected via Lipofectamine 2000® (Invitrogen) according to the manufacturer's protocol.

Transfection of primary neurons. Freshly dissociated cortical neurons were transfected using the Amaxa nucleofector® II (Lonza, Cologne, Germany) using modified manufacturer's protocols. An improved calcium-transfection protocol under ambient CO_2 partial pressure was used to gently transfect mature neurons (Goetze et al., 2004). This technique preserved fine neuronal morphology and survival post-transfection in mature neurons up to DIV21, as observed by us and others (Karra and Dahm, 2010). Transfection efficiencies ranged typically between 5 - 20 %, while triple-vector co-transfection efficiencies were determined using visibly-expressed fluorescent protein at 68 ± 3.84 % (n = 5 wells). The following transfection vectors were used pCMV6-Entry-Myc-FLAG-FHF1b (PCR-amplified and subcloned into pCMV6-Entry from a human cDNA clone; NM_004113.3, Origene), pcDNA4/HisMaxA-NEMO (Fenner et al., 2009), p65-EGFP-N1 (a generous gift of E. Floettmann and M. Rowe, Cardiff, UK), EGFP-N1 (Clontech, Heidelberg, Germany) served to determine positively-tranasfected cells or as control, EB1-GFP (Piehl and Cassimeris, 2003), wild-type & K44M-IKKβ (kinase-dead, Addgene plasmids 11103 and 11104 (Mercurio et al., 1997), wild-type and NEMO-L329P (Addgene plasmids 11970 and 11971; Wu et al., 2006).

Generation of mammalian two-hybrid vectors. Two-hybrid complementation plasmids were generated by ligation into the according vectors as directed by the manufacturer's protocol (CheckMate®, Promega, Southampton, UK).

RNA silencing and quantitative PCR. HuSH-29mer small-hairpin (shRNA) vectors against rat *Nemo/Ikbkg* in pRFP-C-RS, *Fhf1* in pRS and *RelA/p65* in pGFP-V-RS were obtained from Origene (Rockville, MD, USA). Of four targeting vectors, the two most effective sequences were determined by Western-blot (*RelA*) or qPCR (*Ikbkg, Fhf12*). RNA was isolated and its levels were measured by RT-qPCR based on a LightCycler RNA Master SYBR Green I kit (Roche) with a LightCycler 2 instrument, normalized against 18S-rRNA. Measured mRNA amounts were normalized against *18S*-rRNA. Primers used for RT-qPCR were MM-FHF1-FWD (5′-TTCAGCCAGCAGGGATATTT-3′) and MM-FHF1-REV (5′-TCTCCATTCATGGCCACATA-3′) for FHF1, Rn-NEMO-FWD1 (5′-ATGGATCCATGAATAGGCACCTCTGGAAGAGCC-3′) and Rn-NEMO-REV1 (5′- AGGAATTCCTACTCAATGCACTCCATGACATG-3′).

Protein microarray screening. Biotinylated full-length human recombinant NEMO and BSA were used to probe protein microarrays (Invitrogen Protoarray version 4.0) as described previously (Fenner et al., 2010). Significant interactions were identified based on a Z-score cutoff value of 3.0.

Cytosolic extractions. Cytosolic extraction of neurons prior to fixation was performed by incubation of live cells for 3-5 min at 4°C with 1 % (m/v) Triton X-100 in a microtubule-destabilising buffer as described by Robinson et al, 1991 (10 mM Na_3PO_4 pH 7.4, 1 mM $MgCl_2$, 3 mM $CaCl_2$, 150 mM NaCl). Cells were subsequently fixed and immunostained.

Immunofluorescence and microscopy. Primary cultured neurons were fixed in 2 or 4 % paraformaldehyde (PFA). Cells were permeabilized by incubation with ice-cold PBS containing 0.1 % (w/v) Triton X-100 and blocked with 0.3 % (w/v) Triton X-100, 5 % (v/v) horse serum in PBS. They were incubated overnight or weekend at 4°C in primary antibody. The following primary antibodies were used: anti-FHF1 (1:100; Abcam, Cambridge, UK); anti-pIKKα/β (1:500; clone 16A6, Cell Signaling Technology, Hitchin, UK); mouse and rabbit anti-ankyrinG antibodies (1:500; both SCBT, Heidelberg, Germany); mouse monoclonal and rabbit polyclonal anti-NEMO (1:100; FL-419, SCBT, and 1:100; Abcam), anti-EB1 (BD Biosciences, Oxford, UK), anti-PSD-95 (1:250), anti-MAP2 (1:500; both SCBT) and anti-p65 (1:500; active subunit, Millipore). Cultures were incubated for 1 h at RT with secondary antibodies tagged with either Alexa-Fluor 488 nm or Alexa-Fluor 568 nm (1:500, Invitrogen). Photomicrographs were taken using a SPOT RT SE 6 C camera

(Diagnostic Instruments, Sterling Heights, MI, USA) on an Eclipse TE 300 inverted microscope (Nikon, Kingston upon Thames, UK) with Mercury-arc excitation. Confocal images were acquired on a LSM 710 (Zeiss, Jena, Germany) with a DPSS laser diode, an argon, and helium/neon laser and 40x and 63x oil immersion objectives (NA 1.3 and 1.40, Zeiss) at RT. Brain sections: Adult C57BL/6 mice (*mus musculus*) were euthanized by anaesthesia. Brains were removed, post-fixed and cut into 20-50 µm-thick coronal sections. For FHF1-epitope unmasking the free-floating slices were incubated with 0.2 mg/ml pepsin (Dako, Glostrup, Denmark) as described by Lorincz and Nusser, 2008. Co-localization analyses were performed using CoLocalizer Express® software (Japan, Switzerland, Zinchuk and Grossenbacher-Zinchuk, 2011).

Proximity ligation assays. Interactions between neuronal signaling proteins were visualized using pairs of antibodies raised in different species as indicated by Olink Bioscience (Uppsala, Sweden) PLAs using the antibodies as indicated were performed as described in the Duolink manual.

Glutathione-S-transferase (GST) pulldown, co-immunoprecipitation, and Western-blotting. GST-NEMO pulldown and co-immunoprecipitation from lysates of transfected HEK-293T cells expressing FHF1b-FLAG as well as electrophoresis and Western-blotting and immunodetection were performed using standard techniques and as described previously (Fenner et al., 2010). Brain extracts for Western-blotting experiments were prepared using non-ionic-detergent extraction (1 % IGEPAL, Sigma Aldrich) in a sodium/sucrose-buffer. Following brain homogenization the lysate was centrifuged at 27,000 x g at 4 ºC for 20 min. Electrophoresis was performed following volume reduction (Microncon YM-10, Millipore). For determination of IKK-kinase activity, HEK293T cells were transfected with 1 µg of plasmid per dish expressing either empty pEntry vector or pEntry-FHF1-Myc for 24 hours prior to stimulation as indicated. Cells were lysed on ice in 1 mL Tris-based lysis buffer (50 mM Tris-HCl, 150 mM NaCl, 2 mM EDTA, 1% Triton X-100, 1 mM DTT, 1 mM PMSF, 1 µg/mL aprotinin, leupeptin, pepstatin, 1mM Na_3VO_4, 1 mM NaF). Samples were immunoblotted and exposed to anti-phosphorylated IκB (Ser32/36, Cell Signaling Technolgy) antibodies.

Subcellular fractionation of mouse brain extracts. Adult mice were sacrificed and brains immediately removed, homogenized by dounce homogenization in STE-buffer (0.32 M Sucrose, 10 mM Tris-HCl, 1 mM EDTA, pH 7.2), nuclei pelleted by centrifugation (5 min, 1200 g), anti-NeuN (1:1000, Millipore), the cystosole (anti-GAPDH, 1:1000, Millipore) was separated from membrane content by 10 min centrifugation (1200 g), the latter was layered on top of a discontinuous ficoll gradient (7.5% w/v and 10% w/v in STE-buffer) to separate the mitochondrial pellet (anti-Porin,

1:500, Abcam) from the lipid layer (anti-ankyrinG) recovered from the gradient by centrifugation at 28,000 rpm (45 min, Sorvall wx Ultra 100, Fisher Scientific, Dublin, Ireland). Proportionate volumes from the fractions were separated by 6 to 12 % gradient gel electrophoresis. Each fraction marker set was used from a single membrane with two identically loaded membranes used for the different marker proteins.

Ubiquitination Assay. HEK293T cells were seeded at 5×10^5 ml on 10 cm dishes. Dishes were transfected with 1 µg of plasmid encoding NEMO-His, FHF1-Myc and 3 µg of plasmid encoding wildtype HA-Ubiquitin (HA-Ubiq. wt) or plasmids encoding mutant ubiquitin constructs wherein all lysine residues are replaced by arginine residues except at Lys-48 and Lys-63 (HA-Ubiq. R48K and HA-Ubiq. R63K respectively, kindly supplied by Andrew Bowie, Trinity College Dublin) for 24 hours. Ubiquitination of NEMO was assessed using anti-His antibody (1:1000, SCBT). Confirmation of successful transfection of plasmids was determined through immunobloting with anti-Myc (1:2000, Abcam) and anti-HA (1:1000, SCBT).

Luciferase reporter-gene assays for NF-κB and mammalian two-hybrid luciferase assays. Transcriptional activation of p65/NF-κB was monitored using a vector with six tandem repeats of the κB enhancer element upstream of the coding sequence of the firefly-luciferase (NF-κB-luc; P. Baeuerle, Freiburg, Germany) along with a plasmid encoding renilla-luciferase under constitutive thymidin-kinase promoter (phRL-TK-luc; Promega) as a transfection control for normalisation in DUAL-Luciferase® assays. Protein-protein interactions in PC12 cells and neurons were confirmed using the CheckMate®/Flexi mammalian two-hybrid system (Promega, Southampton, UK). Proteins of interest were co-expressed with a GAL4-DNA binding domain (FN11A) and a *herpes simplex*-derived VP16 transcriptional activation domain (FN10A), respectively. Interactions were analysed by measuring firefly-luciferase transcriptional activation downstream of five GAL4-binding sites and a minimal TATA-box as promoter. Expression of renilla-luciferase, encoded under control of a SV40 promoter on the pFN11A vector, was measured as transfection control. Primary cortical neurons were transfected with the indicated plasmids at DIV5. Cells were lysed 48 hours post transfection and DUAL-luciferase assays® were performed as described above.

Sholl plots and high-content analyses of neuronal morphology parameters. Photomicrographs of EGFP or RFP-expressing mature rat hippocampal neurons were taken at 20× magnification (NA 0.45) using an Eclipse TE 300 inverted microscope (Nikon) and the appropriate filter settings as indicated. Coordinates of the branching points plus neurite end-points in relation to the soma were

estimated manually. We used a MATLAB-based algorithm (2007b, Mathworks, Cambridge, UK) to generate the corresponding Sholl profile as described in Gutierrez et al (Gutierrez and Davies, 2007). A L OWESS-algorithm with a smoothing window of 10 points was applied to derive a regression line for the Scholl profile using GraphPad Prism. The region of difference between the profile Sholl sections (points binned within multiplies 20 μm distance) was established and evaluated using Pearson's chi-square test with $p \leq 0.05$ corresponding to the significant difference between the sections. For high content analysis, images from several fields per well were acquired. Neurites were segmented at fixed intensity threshold and delineated using skeletonization of their binary masks. The total neurite length and branching points were normalized to the respective control cells. All image processing operations were executed using Neuronal Profiling BioApplication of the Discovery Toolbox Software (Thermofisher, Horsham, UK). The cells were imaged in 3D (Z-stacks) using using the Zeiss LSM 710. Fluorescence of co-transfected EGFP was excited using 488 nm light and registered in 493–600 nm emission range. The z-stacks were collected with confocal pinhole set to 1.0 Airy unit at the maximum of EGFP emission, which corresponded to approximately 600 nm of optical section thickness. Each dataset contained one neuronal cell, which was segmented based on statistical thresholding (1^{st} percentile of dataset intensity distribution). Neuronal spines were detected using a voxel clustering approach (Rodriguez et al., 2008). The image processing and analysis procedures were executed using Neuron Studio version 0.9.92 (Rodriguez et al., 2006).

Statistics. Statistical analyses and algorithmic procedures were performed using Matlab (MathWorks Inc., Massachusetts, USA), GraphPad Prism (GraphPad Software, Inc., San Diego, USA) or SPSS (IBM, Dublin, Ireland) software suites. Normal distribution of data was tested using Shaprio-Wilk, Kolmogorov-Smirnov or D'Agostino & Pearson omnibus test. Statistical significance was determined using two-tailed student t-tests, one-tailed t-test where applicable on one-tailed hypotheses, or one-way ANOVA followed by Tukey's post-hoc test for normal distribution of data. For non-parametric data, Mann-Whitney or Kruskal-Wallis test was used. Statistical significance defined at the level of $p \leq 0.05$ was marked by asterisks. Bars represent the arithmetic mean ± standard error of the mean (s.e.m.), unless otherwise stated.

Acknowledgements.

The authors thank Heiko Düssmann, Tobias Engel and Caoimhín Concannon for technical discussions and advice. We would further like to thank Sarah Cannon for technical help and Orla Watters for critical reading of the manuscript. This work was supported by Science Foundation Ireland (08/IN.1/B1949), the Higher Education Authority, Ireland (PRTLI Cycle 4), and the European Union (EU FP6-Mobility, Marie Curie Transfer of Knowledge Fellowships and EU FP7-CEMP programme, jointly funded by the National Biophotonics and Imaging Platform, HEA).

References

Albensi, B. C. and Mattson, M. P. (2000). Evidence for the involvement of TNF and NF-kappaB in hippocampal synaptic plasticity. *Synapse* **35**, 151-9.

Barnes, A. P. and Polleux, F. (2009). Establishment of axon-dendrite polarity in developing neurons. *Annu Rev Neurosci* **32**, 347-81.

Berchtold, C. M., Wu, Z. H., Huang, T. T. and Miyamoto, S. (2007). Calcium-dependent regulation of NEMO nuclear export in response to genotoxic stimuli. *Mol Cell Biol* **27**, 497-509.

Bhakar, A. L., Tannis, L. L., Zeindler, C., Russo, M. P., Jobin, C., Park, D. S., MacPherson, S. and Barker, P. A. (2002). Constitutive nuclear factor-kappa B activity is required for central neuron survival. *J Neurosci* **22**, 8466-75.

Buchser, W. J., Slepak, T. I., Gutierrez-Arenas, O., Bixby, J. L. and Lemmon, V. P. (2010). Kinase/phosphatase overexpression reveals pathways regulating hippocampal neuron morphology. *Mol Syst Biol* **6**, 391.

Chiarugi, A. (2002). Characterization of the molecular events following impairment of NF-kappaB-driven transcription in neurons. *Brain Res Mol Brain Res* **109**, 179-88.

Dotti, C. G., Sullivan, C. A. and Banker, G. A. (1988). The establishment of polarity by hippocampal neurons in culture. *J Neurosci* **8**, 1454-68.

Fenner, B. J., Scannell, M. and Prehn, J. H. (2009). Identification of polyubiquitin binding proteins involved in NF-kappaB signaling using protein arrays. *Biochim Biophys Acta* **1794**, 1010-6.

Fenner, B. J., Scannell, M. and Prehn, J. H. (2010). Expanding the substantial interactome of NEMO using protein microarrays. *PLoS One* **5**, e8799.

Fridmacher, V., Kaltschmidt, B., Goudeau, B., Ndiaye, D., Rossi, F. M., Pfeiffer, J., Kaltschmidt, C., Israel, A. and Memet, S. (2003). Forebrain-specific neuronal inhibition of nuclear factor-kappaB activity leads to loss of neuroprotection. *J Neurosci* **23**, 9403-8.

Gautheron, J. and Courtois, G. (2010). "Without Ub I am nothing": NEMO as a multifunctional player in ubiquitin-mediated control of NF-kappaB activation. *Cellular and molecular life sciences : CMLS* **67**, 3101-13.

Goetz, R., Dover, K., Laezza, F., Shtraizent, N., Huang, X., Tchetchik, D., Eliseenkova, A. V., Xu, C. F., Neubert, T. A., Ornitz, D. M. et al. (2009). Crystal structure of a fibroblast growth factor homologous factor (FHF) defines a conserved surface on FHFs for binding and modulation of voltage-gated sodium channels. *J Biol Chem* **284**, 17883-96.

Goetze, B., Grunewald, B., Baldassa, S. and Kiebler, M. (2004). Chemically controlled formation of a DNA/calcium phosphate coprecipitate: application for transfection of mature hippocampal neurons. *J Neurobiol* **60**, 517-25.

Goldfarb, M. (2005). Fibroblast growth factor homologous factors: evolution, structure, and function. *Cytokine Growth Factor Rev* **16**, 215-20.

Goldfarb, M., Schoorlemmer, J., Williams, A., Diwakar, S., Wang, Q., Huang, X., Giza, J., Tchetchik, D., Kelley, K., Vega, A. et al. (2007). Fibroblast growth factor homologous factors control neuronal excitability through modulation of voltage-gated sodium channels. *Neuron* **55**, 449-63.

Gutierrez, H. and Davies, A. M. (2007). A fast and accurate procedure for deriving the Sholl profile in quantitative studies of neuronal morphology. *J Neurosci Methods* **163**, 24-30.

Gutierrez, H., Hale, V. A., Dolcet, X. and Davies, A. (2005). NF-kappaB signalling regulates the growth of neural processes in the developing PNS and CNS. *Development* **132**, 1713-26.

Hedstrom, K. L., Ogawa, Y. and Rasband, M. N. (2008). AnkyrinG is required for maintenance of the axon initial segment and neuronal polarity. *J Cell Biol* **183**, 635-40.

Henn, I. H., Bouman, L., Schlehe, J. S., Schlierf, A., Schramm, J. E., Wegener, E., Nakaso, K., Culmsee, C., Berninger, B., Krappmann, D. et al. (2007). Parkin mediates neuroprotection through activation of IkappaB kinase/nuclear factor-kappaB signaling. *J Neurosci* **27**, 1868-78.

Imielski, Y., Schwamborn, J. C., Luningschror, P., Heimann, P., Holzberg, M., Werner, H., Leske, O., Puschel, A. W., Memet, S., Heumann, R. et al. (2012). Regrowing the adult brain: NF-kappaB controls functional circuit formation and tissue homeostasis in the dentate gyrus. *PLoS One* **7**, e30838.

Kaltschmidt, B. and Kaltschmidt, C. (2009). NF-kappaB in the nervous system. *Cold Spring Harb Perspect Biol* **1**, a001271.

Kaltschmidt, C., Kaltschmidt, B. and Baeuerle, P. A. (1995). Stimulation of ionotropic glutamate receptors activates transcription factor NF-kappa B in primary neurons. *Proc Natl Acad Sci U S A* **92**, 9618-22.

Kaltschmidt, C., Kaltschmidt, B., Neumann, H., Wekerle, H. and Baeuerle, P. A. (1994). Constitutive NF-kappa B activity in neurons. *Mol Cell Biol* **14**, 3981-92.

Karra, D. and Dahm, R. (2010). Transfection techniques for neuronal cells. *J Neurosci* **30**, 6171-7.

König, H. G., Kögel, D., Rami, A. and Prehn, J. H. (2005). TGF-{beta}1 activates two distinct type I receptors in neurons: implications for neuronal NF-{kappa}B signaling. *J Cell Biol* **168**, 1077-86.

Laezza, F., Gerber, B. R., Lou, J. Y., Kozel, M. A., Hartman, H., Craig, A. M., Ornitz, D. M. and Nerbonne, J. M. (2007). The FGF14(F145S) mutation disrupts the interaction of FGF14 with voltage-gated Na+ channels and impairs neuronal excitability. *J Neurosci* **27**, 12033-44.

Laezza, F., Lampert, A., Kozel, M. A., Gerber, B. R., Rush, A. M., Nerbonne, J. M., Waxman, S. G., Dib-Hajj, S. D. and Ornitz, D. M. (2009). FGF14 N-terminal splice variants differentially modulate Nav1.2 and Nav1.6-encoded sodium channels. *Mol Cell Neurosci* **42**, 90-101.

Li, J., Gu, X., Ma, Y., Calicchio, M. L., Kong, D., Teng, Y. D., Yu, L., Crain, A. M., Vartanian, T. K., Pasqualini, R. et al. (2010). Nna1 mediates Purkinje cell dendritic development via lysyl oxidase propeptide and NF-kappaB signaling. *Neuron* **68**, 45-60.

Lilienbaum, A. and Israel, A. (2003). From calcium to NF-kappa B signaling pathways in neurons. *Mol Cell Biol* **23**, 2680-98.

Lorincz, A. and Nusser, Z. (2008). Cell-type-dependent molecular composition of the axon initial segment. *J Neurosci* **28**, 14329-40.

Lou, J. Y., Laezza, F., Gerber, B. R., Xiao, M., Yamada, K. A., Hartmann, H., Craig, A. M., Nerbonne, J. M. and Ornitz, D. M. (2005). Fibroblast growth factor 14 is an intracellular modulator of voltage-gated sodium channels. *J Physiol* **569**, 179-93.

Makris, C., Roberts, J. L. and Karin, M. (2002). The carboxyl-terminal region of IkappaB kinase gamma (IKKgamma) is required for full IKK activation. *Mol Cell Biol* **22**, 6573-81.

Meffert, M. K., Chang, J. M., Wiltgen, B. J., Fanselow, M. S. and Baltimore, D. (2003). NF-kappa B functions in synaptic signaling and behavior. *Nat Neurosci* **6**, 1072-8.

Mercurio, F., Zhu, H., Murray, B. W., Shevchenko, A., Bennett, B. L., Li, J., Young, D. B., Barbosa, M., Mann, M., Manning, A. et al. (1997). IKK-1 and IKK-2: cytokine-activated IkappaB kinases essential for NF-kappaB activation. *Science* **278**, 860-6.

Mikenberg, I., Widera, D., Kaus, A., Kaltschmidt, B. and Kaltschmidt, C. (2007). Transcription factor NF-kappaB is transported to the nucleus via cytoplasmic dynein/dynactin motor complex in hippocampal neurons. *PLoS One* **2**, e589.

Nakamori, Y., Emoto, M., Fukuda, N., Taguchi, A., Okuya, S., Tajiri, M., Miyagishi, M., Taira, K., Wada, Y. and Tanizawa, Y. (2006). Myosin motor Myo1c and its receptor NEMO/IKK-gamma promote TNF-alpha-induced serine307 phosphorylation of IRS-1. *J Cell Biol* **173**, 665-71.

Nakata, T. and Hirokawa, N. (2003). Microtubules provide directional cues for polarized axonal transport through interaction with kinesin motor head. *J Cell Biol* **162**, 1045-55.

O'Sullivan, N. C., Croydon, L., McGettigan, P. A., Pickering, M. and Murphy, K. J. (2010). Hippocampal region-specific regulation of NF-kappaB may contribute to learning-associated synaptic reorganisation. *Brain Res Bull* **81**, 385-90.

Olsen, S. K., Garbi, M., Zampieri, N., Eliseenkova, A. V., Ornitz, D. M., Goldfarb, M. and Mohammadi, M. (2003). Fibroblast growth factor (FGF) homologous factors share structural but not functional homology with FGFs. *J Biol Chem* **278**, 34226-36.

Perkins, N. D. (2006). Post-translational modifications regulating the activity and function of the nuclear factor kappa B pathway. *Oncogene* **25**, 6717-30.

Piehl, M. and Cassimeris, L. (2003). Organization and dynamics of growing microtubule plus ends during early mitosis. *Mol Biol Cell* **14**, 916-25.

Ramakrishna, S., Suresh, B., Lee, E. J., Lee, H. J., Ahn, W. S. and Baek, K. H. (2011). Lys-63-specific deubiquitination of SDS3 by USP17 regulates HDAC activity. *The Journal of biological chemistry* **286**, 10505-14.

Rasband, M. N. (2010). The axon initial segment and the maintenance of neuronal polarity. *Nat Rev Neurosci* **11**, 552-62.

Rodriguez, A., Ehlenberger, D. B., Dickstein, D. L., Hof, P. R. and Wearne, S. L. (2008). Automated three-dimensional detection and shape classification of dendritic spines from fluorescence microscopy images. *PLoS One* **3**, e1997.

Rodriguez, A., Ehlenberger, D. B., Hof, P. R. and Wearne, S. L. (2006). Rayburst sampling, an algorithm for automated three-dimensional shape analysis from laser scanning microscopy images. *Nat Protoc* **1**, 2152-61.

Rothwarf, D. M., Zandi, E., Natoli, G. and Karin, M. (1998). IKK-gamma is an essential regulatory subunit of the IkappaB kinase complex. *Nature* **395**, 297-300.

Russo, S. J., Wilkinson, M. B., Mazei-Robison, M. S., Dietz, D. M., Maze, I., Krishnan, V., Renthal, W., Graham, A., Birnbaum, S. G., Green, T. A. et al. (2009). Nuclear factor kappa B signaling regulates neuronal morphology and cocaine reward. *J Neurosci* **29**, 3529-37.

Sanchez-Ponce, D., Tapia, M., Munoz, A. and Garrido, J. J. (2008). New role of IKK alpha/beta phosphorylated I kappa B alpha in axon outgrowth and axon initial segment development. *Mol Cell Neurosci* **37**, 832-44.

Schafer, D. P., Jha, S., Liu, F., Akella, T., McCullough, L. D. and Rasband, M. N. (2009). Disruption of the axon initial segment cytoskeleton is a new mechanism for neuronal injury. *J Neurosci* **29**, 13242-54.

Schmidt-Ullrich, R., Memet, S., Lilienbaum, A., Feuillard, J., Raphael, M. and Israel, A. (1996). NF-kappaB activity in transgenic mice: developmental regulation and tissue specificity. *Development* **122**, 2117-28.

Schmukle, A. C. and Walczak, H. (2012). No one can whistle a symphony alone - how different ubiquitin linkages cooperate to orchestrate NF-kappaB activity. *Journal of cell science* **125**, 549-59.

Schultz, C., König, H. G., Del Turco, D., Politi, C., Eckert, G. P., Ghebremedhin, E., Prehn, J. H., Kögel, D. and Deller, T. (2006). Coincident enrichment of phosphorylated IkappaBalpha, activated IKK, and phosphorylated p65 in the axon initial segment of neurons. *Mol Cell Neurosci* **33**, 68-80.

Segal, M. (2010). Dendritic spines, synaptic plasticity and neuronal survival: activity shapes dendritic spines to enhance neuronal viability. *Eur J Neurosci* **31**, 2178-84.

Smallwood, P. M., Munoz-Sanjuan, I., Tong, P., Macke, J. P., Hendry, S. H., Gilbert, D. J., Copeland, N. G., Jenkins, N. A. and Nathans, J. (1996). Fibroblast growth factor (FGF) homologous factors: new members of the FGF family implicated in nervous system development. *Proc Natl Acad Sci U S A* **93**, 9850-7.

Sobotzik, J. M., Sie, J. M., Politi, C., Del Turco, D., Bennett, V., Deller, T. and Schultz, C. (2009). AnkyrinG is required to maintain axo-dendritic polarity in vivo. *Proc Natl Acad Sci U S A* **106**, 17564-9.

Soderberg, O., Gullberg, M., Jarvius, M., Ridderstrale, K., Leuchowius, K. J., Jarvius, J., Wester, K., Hydbring, P., Bahram, F., Larsson, L. G. et al. (2006). Direct observation of individual endogenous protein complexes in situ by proximity ligation. *Nat Methods* **3**, 995-1000.

Solt, L. A., Madge, L. A. and May, M. J. (2009). NEMO-binding domains of both IKKalpha and IKKbeta regulate IkappaB kinase complex assembly and classical NF-kappaB activation. *J Biol Chem* **284**, 27596-608.

Tang, E. D., Wang, C. Y., Xiong, Y. and Guan, K. L. (2003). A role for NF-kappaB essential modifier/IkappaB kinase-gamma (NEMO/IKKgamma) ubiquitination in the activation of the IkappaB kinase complex by tumor necrosis factor-alpha. *J Biol Chem* **278**, 37297-305.

van Loo, G., De Lorenzi, R., Schmidt, H., Huth, M., Mildner, A., Schmidt-Supprian, M., Lassmann, H., Prinz, M. R. and Pasparakis, M. (2006). Inhibition of transcription factor NF-kappaB in the central nervous system ameliorates autoimmune encephalomyelitis in mice. *Nat Immunol* **7**, 954-61.

van Swieten, J. C., Brusse, E., de Graaf, B. M., Krieger, E., van de Graaf, R., de Koning, I., Maat-Kievit, A., Leegwater, P., Dooijes, D., Oostra, B. A. et al. (2003). A mutation

in the fibroblast growth factor 14 gene is associated with autosomal dominant cerebellar ataxia [corrected]. *Am J Hum Genet* **72**, 191-9.

Wang, C., Hoch, E. G. and Pitt, G. S. (2011). Identification of novel interaction sites that determine specificity between fibroblast growth factor homologous factors and voltage-gated sodium channels. *The Journal of biological chemistry* **286**, 24253-63.

Wang, Q., Bardgett, M. E., Wong, M., Wozniak, D. F., Lou, J., McNeil, B. D., Chen, C., Nardi, A., Reid, D. C., Yamada, K. et al. (2002). Ataxia and paroxysmal dyskinesia in mice lacking axonally transported FGF14. *Neuron* **35**, 25-38.

Winckler, B., Forscher, P. and Mellman, I. (1999). A diffusion barrier maintains distribution of membrane proteins in polarized neurons. *Nature* **397**, 698-701.

Windheim, M., Peggie, M. and Cohen, P. (2008). Two different classes of E2 ubiquitin-conjugating enzymes are required for the mono-ubiquitination of proteins and elongation by polyubiquitin chains with a specific topology. *Biochem J* **409**, 723-9.

Wu, C. J., Conze, D. B., Li, T., Srinivasula, S. M. and Ashwell, J. D. (2006). Sensing of Lys 63-linked polyubiquitination by NEMO is a key event in NF-kappaB activation [corrected]. *Nature cell biology* **8**, 398-406.

Xiao, M., Xu, L., Laezza, F., Yamada, K., Feng, S. and Ornitz, D. M. (2007). Impaired hippocampal synaptic transmission and plasticity in mice lacking fibroblast growth factor 14. *Mol Cell Neurosci* **34**, 366-77.

Yamaoka, S., Courtois, G., Bessia, C., Whiteside, S. T., Weil, R., Agou, F., Kirk, H. E., Kay, R. J. and Israel, A. (1998). Complementation cloning of NEMO, a component of the IkappaB kinase complex essential for NF-kappaB activation. *Cell* **93**, 1231-40.

Zinchuk, V. and Grossenbacher-Zinchuk, O. (2011). Quantitative colocalization analysis of confocal fluorescence microscopy images. *Current protocols in cell biology*. **Chapter 4**, Unit4 19.

Zonta, B., Desmazieres, A., Rinaldi, A., Tait, S., Sherman, D. L., Nolan, M. F. and Brophy, P. J. (2011). A critical role for Neurofascin in regulating action potential initiation through maintenance of the axon initial segment. *Neuron* **69**, 945-56.

Figure legends

Figure 1. Interaction between NEMO and FHF1b on protein microarrays and in mammalian cells. (A) Representative images of a subarray portion of protein microarrays probed with labeled BSA and rhNEMO. Alexa Fluor 647 (AF647), biotin and calmodulin 2 (CALM2, a known NEMO interactor) controls (Ctrl) are highlighted. Note the labeled-NEMO, but not labeled-BSA fluorescence on the FHF1b array spots in the middle right of the subarray. **(B)** NEMO displays significant interaction with full-length FHF1b on protein microarrays. Average Z scores ± S.D. from two arrays, obtained when NEMO or BSA (control) were used to probe microarrays, are shown for FHF1b and the canonical NEMO partners IKKα and IKKβ (compare Suppl. Fig. 1). **(C)** HEK293 cells were transfected with myc-tagged FHF1b and Xpress-tagged NEMO (pNEMO) or plasmid control (pEmpty). Xpress-tagged NEMO (NEMO plasmid, pNEMO) was immunoprecipitated with anti-XPress as indicated and co-immunoprecipitated myc-FHF1b was detected with anti-myc (lane 4). Only a small amount of FHF1b was detected in immunoprecipitates derived from empty Xpress vector lysates (pEmpty, lane 3). **(D)** Pulldown of GST-tagged NEMO results in co-pulldown of FHF1b in HEK293 cells, minimal co-pulldown using GST control. FHF1b and NEMO associate in **(E)** PC12 cells and **(F)** cortical neurons in a two-hybrid assay. Transcriptional activation of the interaction-specific firefly luciferase reporter was monitored in living cells transfected with empty Act/Bind vectors (Vector/Vector), positive control MyoD/Id vectors, NEMO/Bind vectors (NEMO/Vector), Act/FHF1b vectors (Vector/FHF1b) and NEMO/FHF1b vectors after 24 hours and normalized to constitutive renilla-luciferase expression (n = 6, ± S.D., *p≤0.05).

Figure 2. FHF1 is expressed in the axon initial segment of neurons in vitro and in vivo. (A) Immunoreactivity against endogenous FHF1-protein in the AIS. Cortical neuronal cultures were maintained for three weeks in vitro before being subjected to immunofluorescence analyses. Confocal laser scanning microscopy (C-LSM) analysis illustrates co-localization of FHF1 immunoreactivity (red) to the ankyrinG positive AIS (AnkG, green, arrows, Hoechst-staining in blue). Experiments were repeated with comparable results. **(B)** Mature neurons were transfected using pCMV6-Entry-FHF1b (FHF1) and pEGFP and labeled with mouse anti-FHF1 antibody. Marked immunoreactivity in transfected neurons is depicted. Experiments were repeated twice with comparable results. **(C)** Immunoreactivity using the anti-FHF1 antibody in mature cultured neurons transfected with control vector and EGFP reveals its location along the AIS (red, arrow). Note the reduction in anti-FHF1 immunofluorescence along the proximal axon (arrow in C; C', n = 11 - 22 EGFP-positive cells, p = 0.017, one-tailed t-test) and reduced total somatic anti-FHF1

immunofluorescence (C'', p = 0.119) five days following transfection of cortical neurons using the pooled small hairpin constructs directed against *Fhf1*. The experiment was repeated with comparable results. **(D)** Freshly-isolated adult cortical tissue was homogenized in IGEPAL-CA-630/sucrose buffer followed by Western-blot analyses. FHF1-immunoreactivity and ankyrinG in the lysates is depicted. **(E-G)** In situ immunofluorescence analyses of FHF1 expression in adult mouse brain slices. FHF1 epitope-retrieval was achieved by pepsin/HCl pre-treatment on floating sections, **(F)** depicts untreated slice as negative control. Identification of positive co-localization of FHF1 immunoreactivity to the ankyrinG-positive AIS in the cortex **(E)** and hippocampus (close-up of dentage gyrus in **G**) was achieved by C-LSM. Experiments were repeated twice with comparable results. Scale bars, 10 µm; 5 µm in (G).

Figure 3. FHF1, NEMO and pIKKα/β co-localise in the AIS membrane. (A,B) Living adult cortical neurons were cold-detergent-extracted for 3 minutes directly followed by fixation using paraformaldehyde. Anti-FHF1 (A) or anti-pan-NEMO (B) immunofluorescence in the AIS (arrows) is depicted versus AnkyrinG immunofluorescence (green). Images acquired from confocal stack analysis depicted in Suppl. Fig. 3B , C. Experiments were repeated once with comparable results. **(C,C')** Dimished immunoreactivity against phosphorylated IKKα/β (pIKKα/β, green) in the AIS following NEMO silencing. Integrated AIS immunofluorescence intensity was determined following a four day transfection period with pRS-C-RFP-shRNA (RFP, red fluorescent protein) constructs, directed against *NEMO* mRNA or scrambled control (arrows, C', n = 16 - 17, p = 0.04). Scale bars, 20 µm. (Efficiency of RNAi constructs is depicted in Suppl. Fig. 2A-D). **(D,E)** Neurons were maintained for three weeks in vitro before being subjected to immunofluorescence analyses. Confocal laser scanning microscopy (C-LSM) analysis illustrates immunoreactivity against phosphorylated-IKKα/β (green) and FHF1 (red) co-localising to the AIS (arrows). Pixels corresponding to the highest immunoreactivity intensities (upper quadrant of the scatter-gram) against both, FHF1 and pIKKα/β, as quantitated by CoLocalizer express® software, predominate mainly in axon initial segments (co-localizing pixels depicted in white, binary image generated by CoLocalizer). Scale bars in D, 10 µm; 5 µm in E. (**F**) Extracts from adult brain cortical tissue were collected by homogenization in sucrose-buffer and subsequently fractionated using a 7.5 % - 10 % Ficoll gradient. Pellets and supernatants corresponding to nuclear, cytosolic (including extracellular fluid/ECF), mitochondria and lipid fractions were collected, and corresponding volume fractions were subjected to Western-blot analyses. Antibodies raised against GAPDH (cytosol), NeuN (nucleus), Porin (mitochondria) and AnkyrinG (lipid membrane) served to confirm the fractionation process.

Figure 4. *In situ* proximity ligation assay (PLA) reveal FHF1 / IKK-complex interaction in the AIS. (A) Schematic representation of the *in situ* proximity ligation assay. Amplification of the fluorescent probe is achieved when oligonucleotides reach proximity ≤ 40 nm. **(B-I)** Proximity ligation mediated between overexpressed **(B-D)** and endogenous **(H-I)** epitopes of FHF1 and NEMO: Analysis 24 h following transfection of primary neurons with both NEMO/FHF1b **(B,C)** or FHF1b **(D)** or NEMO **(E)** vectors. Following exposure to mouse anti-FHF1 and rabbit anti-NEMO antibodies, PLA was performed. Red spots indicate amplified detection of fluorescently-labeled oligonucleotides at locations of molecular proximity between epitopes (nuclei in blue; asterisk, cell bodies of transfected cells). **(E,F)** Mature neurons were transfected with NEMO vector (pNEMO), or the AIS-microtubule marker pEB1-GFP as indicated, detergent-extracted and fixed 72 h following transfection. Subsequent PLA using FHF1/NEMO antibody pairs to reveal interactions in the detergent-resistant cytoskeleton, using pan-IKKβ/EB1 antibody pairs as negative control (F), were performed. Post PLA anti-ankyrinG staining served to highlight the location of the AIS. Note the pronounced enrichment of PLA-spots along the ankG-positive AIS (arrows in E,J) and their significantly reduced numbers in EB1-GFP positive AIS's (**G**, n = 10 - 12). **(H-K)** Proximity ligation between the endogenous epitopes of FHF1 and either members of the IKK complex: NEMO **(H,J)** or pan-IKKβ **(I)**. Note the accumulation of fluorescent oligonucleotides along a prototypical 20-50 µm stretch reminiscent of the location of the axon-initial segment (arrows). Subsequent immunofluorescence analysis revealed proximity ligation (arrows, red spots) along the ankyrinG positive stretch (**J**, green). **(K)** Parallel mature cultures were kept for three weeks in culture before detergent extraction, fixation and PLA-assays. They were then co-labelled with ankG (AIS), the somato-dendritic marker MAP-2 or the post-synaptic density marker PSD-95 (Suppl. Fig. 3). PLA-spots in the respective compartments were counted (7-33 photomicrographs from 4 wells). **(L)** Transfected neurons exposed to antibodies raised against NEMO and pan-IKKβ served as positive control for the proximity ligation assay. **(M)** Lack of proximity ligation in non-transfected neurons exposed to anti-FLAG or anti-XPress antibodies. Experiments in B-D, H-I, M were replicated with comparable results. Scale bars, 10 µm; 50 µm in (B), 5 µm in (C-D, H-I, L-M), 2 µm in (J)**.**

Figure 5. NEMO's K63- and K48-linked ubiquitination status is reduced in the presence of FHF1b. (A) HEK293 cells were transfected using FHF1b-Myc or Entry control vectors and stimulated with lipopolysaccharide (LPS, 1 µg/mL) for 30 minutes. Protein lysates were collected and subjected to Western-blot analyses. Anti-phosphorylated Ser32,36 - IκBα, pan-IκBα, as well as anti-Myc immunoreactivities are depicted, an unspecific band and β-Actin served as loading controls. **(B,C)** HEK293 cells were transfected using HA-tagged wild-type ubiquitin (B), HA-

tagged R48K-ubiquitin or HA-tagged R63K-ubiquitin (C), and His-tagged NEMO and Myc-tagged FHF1b together with their respective control vectors as indicated (-, control vector, +, protein-coding vector). Lysates were collected following 24 hours of transfection and subjected to Western-blot analyses. Note the laddering in the anti-His (anti-Myc) immunoreactivity profile indicating polyubiquitination levels of the overexpressed NEMO (FHF1b) proteins. **(D)** Mature cortical neurons were transfected using either control vector (pEntry) or pCMV-FHF1b-Myc. Cells were lysed following two days of transfection and lysates were subjected to Western-blot analyses. Immunoreactivity against NEMO and p65/NF-κB was determined using the respective antibodies. FHF1b expression was verified using anti-Myc antibodies. EGFP co-transfection served to monitor transfection efficiency and α-Tubulin served as loading control.

Figure 6. FHF1-silencing in mature neurons is a potent inducer of NF-κB-dependent transcriptional activation in a NEMO-dependent manner. (A) Primary cortical neurons were cultured for 4, 7, 12 or 18-days in vitro (DIV), respectively. Cells were immediately fixed for 12 minutes followed by immunoabelling using the antibodies as indicated and photomicrographs were aquired by C-LSM using constant laser power and pinhole settings (anti-FHF1, green; anti-AnkyrinG, red). Note the increase in FHF1-expression and compartmentalization over time. **(B)** Mature neurons were transfected with FHF1b-expresssion vector as indicated (B), and κB-firefly luciferase and constitutive renilla-luciferase vectors. Dual-luciferase assays were performed to determine relative κB-dependent reporter gene activity (48 hours). **(C)** Immature neurons were transfected on day four in vitro with vectors encoding *Fhf1*-directed small-hairpin oligonucleotides and κB-reporter. Cells were lysed on day seven and dual-luciferase assays conducted. **(D,E)** shRNA-mediated silencing of *Fhf1, Ikbg*/*Nemo* and *p65* mRNA in mature cortical neurons and resultant NF-κB activity is depicted. Mature neurons were transfected as indicated from day 15 to 19 in vi tro and Dual-luciferase assays performed as above. (Bar graphs depict normalized κB-dependent firefly-luciferase activity (D) n = 12, $p \leq 0.0001$, (E) n = 8-12 wells, $^*p \leq 0.05$, compare Suppl. Fig. 5B,C). **(F)** Mature cortical neurons were transfected with the NF-κB-reporter as above together with the FHF1b expression vector and increasing amounts of either wild-type NEMO vector (0, 0.05, 1, 2.5 μg/well, respectively) or dominant-negative NEMO-L329P (2.5 μg/well, 48 hours), Bar graphs depict κB-dependent luciferase activity (n = 4, $^*p \leq 0.05$)). **(G,H)** Real-time PCR confirms effective co-silencing efficiency of *Fhf1* and *Nemo* mRNA following nucleofection. At DIV7 qPCR analysis for *Nemo* or *Fhf1*-transcripts, respectively was normalized to *18S* rRNA-expression. Scale bars, 10 μm

Figure 6. Maintenance of neuronal morphology depends on constitutive NEMO and p65 activity. FHF1 modulates neuronal morphology in a NEMO-dependent manner. (A, B, G) Sholl-plots at 10 µm increments and Lowess regression line-traces were generated using an algorithm from manually evaluated positions of neurite branching points and termini as input, derived after three (A, n = 27-38 neurons, $p \leq 0.05$: 50-320 µm, chi-square), or five-day knockdown (B: n = 25-34 neurons, $p \leq 0.05$: 100-160 µm; G: n = 20-22, $p \leq 0.05$: 30-190 µm) of the proteins as indicated from EGFP co-transfected mature cortical neurons. (A', B', G' rel. branching point counts from automated image tracing analyses of the respective populations; Neuronal Profiling Bioapplication®). **(C-E)** Normalized results obtained by high content image analysis on average neurite lengths and branching points from mature cortical neurons transfected for five days (DIV15-20) as indicated (n = 396-778). Representative photomicrographs are depicted in (C,**F**). **(H-J)** Freshly-isolated cortical neurons were 'nucleofected' with the indicated plasmids as depicted and maintained for five days. High-content image analyses were then performed on photomicrographs obtained and parameters, as indicated, were normalized to their respective controls for comparison (n = 2041 - 2370 transfected neurons, $*p \leq 0.05$). Scale bars, 20 µm.

Figure 7. FHF1-silencing results in increased spine densities. Mature cortical neurons were co-transfected with EGFP and shRNA-constructs directed against *Fhf1* mRNA for a period of five days. Confocal laser-scanning images at high magnification (63x) were obtained followed by 3D-rendering and algorithmical optical stack analysis. **(A)** Representative renderings of control and FHF1 shRNA transfected neurons are depicted. Scale bar, 10 µm. **(B-E)** Algorithmic determination (Neuron Studio) of overall neurite lengths per unit volume (B, n = 7, p = 0.142), as well as the average spine counts per unit volume (D, n = 7, p = 0.021) or per one-hundred µm of neurite shaft (E, n = 7, p = 0.0013) are depicted together with a prototypical stretch of a spine-studded neurite shaft (C), scale bar 10 µm.

Supplementary Material.

Suppl. Fig. 1: The interaction between FHF1b and NEMO on Invitrogen Protoarrays ranges among the strongest hits on the chip.

Suppl. Fig. 2: Efficiency of shRNA-silencing constructs directed at *Nemo*, *Fhf1* and *p65* mRNA.

Suppl. Fig. 3: Confirmation of specificity for anti-FHF1, anti-NEMO and anti-phosphorylated IKKβ immunofluorescence reactions.

Suppl. Fig. 4: NEMO / FHF1-interactions occur preferentially within the axon-initial segment cytoskeleton.

Suppl. Fig. 5: Profile of active p65/NF-κB during in vitro development and evidence that the activation of NF-κB following *Fhf1*-silencing is sequence specific.

Figure 1

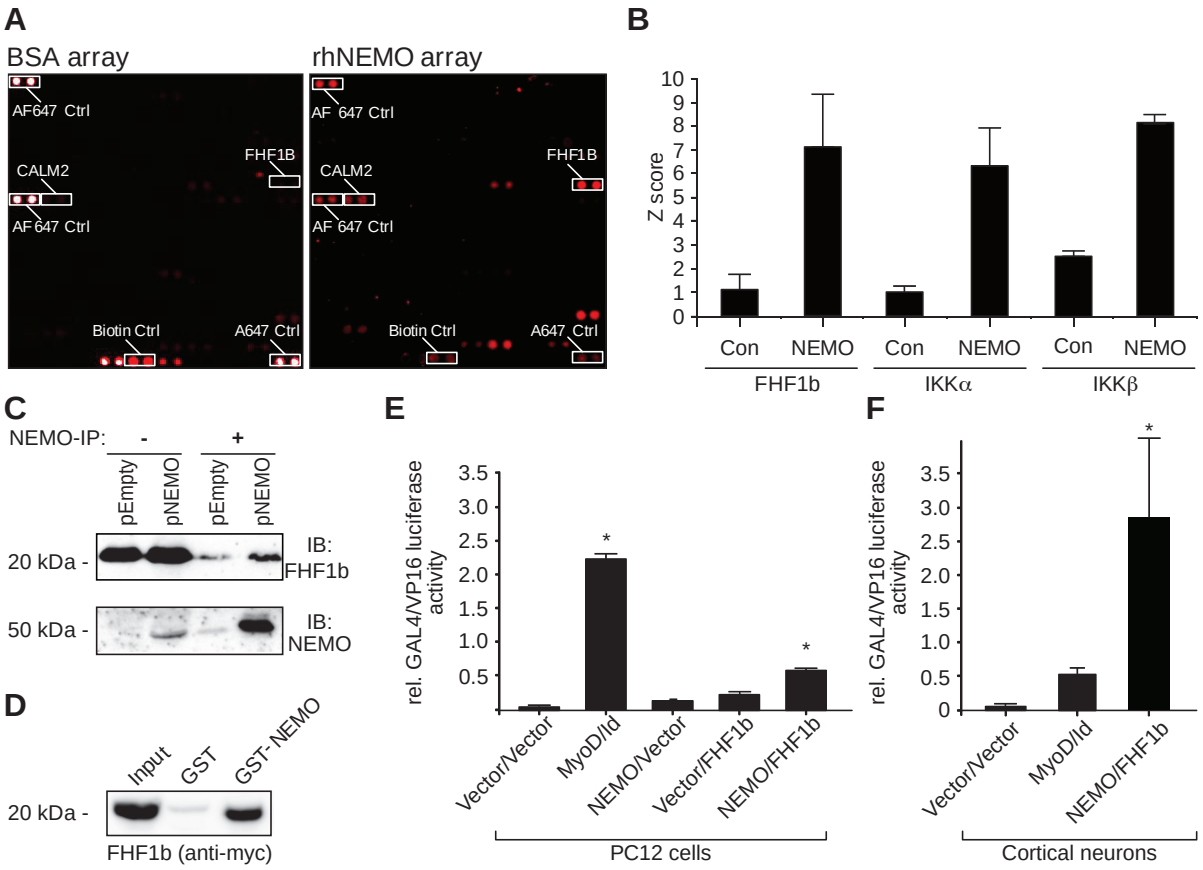
A
BSA array
rhNEMO array
AF647 Ctrl
CALM2
FHF1B
AF647 Ctrl
Biotin Ctrl
A647 Ctrl
AF 647 Ctrl
B
Z score
Con
NEMO
FHF1b
IKKα
IKKβ
C
NEMO-IP:
pEmpty
pNEMO
20 kDa -
IB: FHF1b
50 kDa -
IB: NEMO
D
Input
GST
GST-NEMO
20 kDa -
FHF1b (anti-myc)
E
rel. GAL4/VP16 luciferase activity
Vector/Vector
MyoD/Id
NEMO/Vector
Vector/FHF1b
NEMO/FHF1b
PC12 cells
F
Cortical neurons

Figure 2

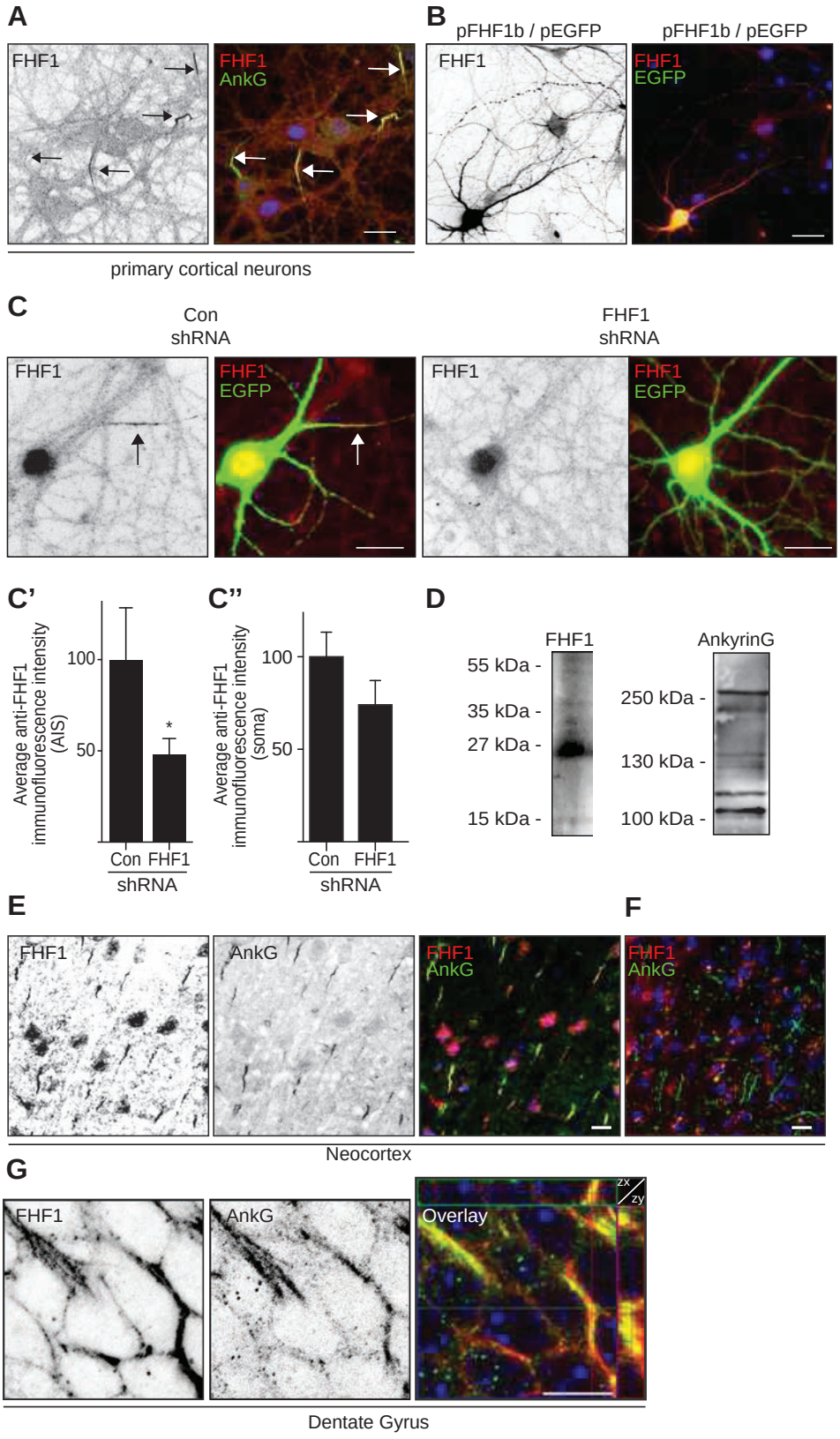
A
FHF1
FHF1
AnkG
primary cortical neurons
B
pFHF1b / pEGFP
pFHF1b / pEGFP
FHF1
FHF1
EGFP
C
Con
shRNA
FHF1
shRNA
FHF1
FHF1
EGFP
FHF1
FHF1
EGFP
C'
Average anti-FHF1 immunofluorescence intensity (AIS)
100
50
*
Con
FHF1
shRNA
C''
Average anti-FHF1 immunofluorescence intensity (soma)
100
50
Con
FHF1
shRNA
D
FHF1
AnkyrinG
55 kDa -
35 kDa -
27 kDa -
15 kDa -
250 kDa -
130 kDa -
100 kDa -
E
F
FHF1
AnkG
FHF1
AnkG
FHF1
AnkG
Neocortex
G
FHF1
AnkG
Overlay
zx
zy
Dentate Gyrus

Figure

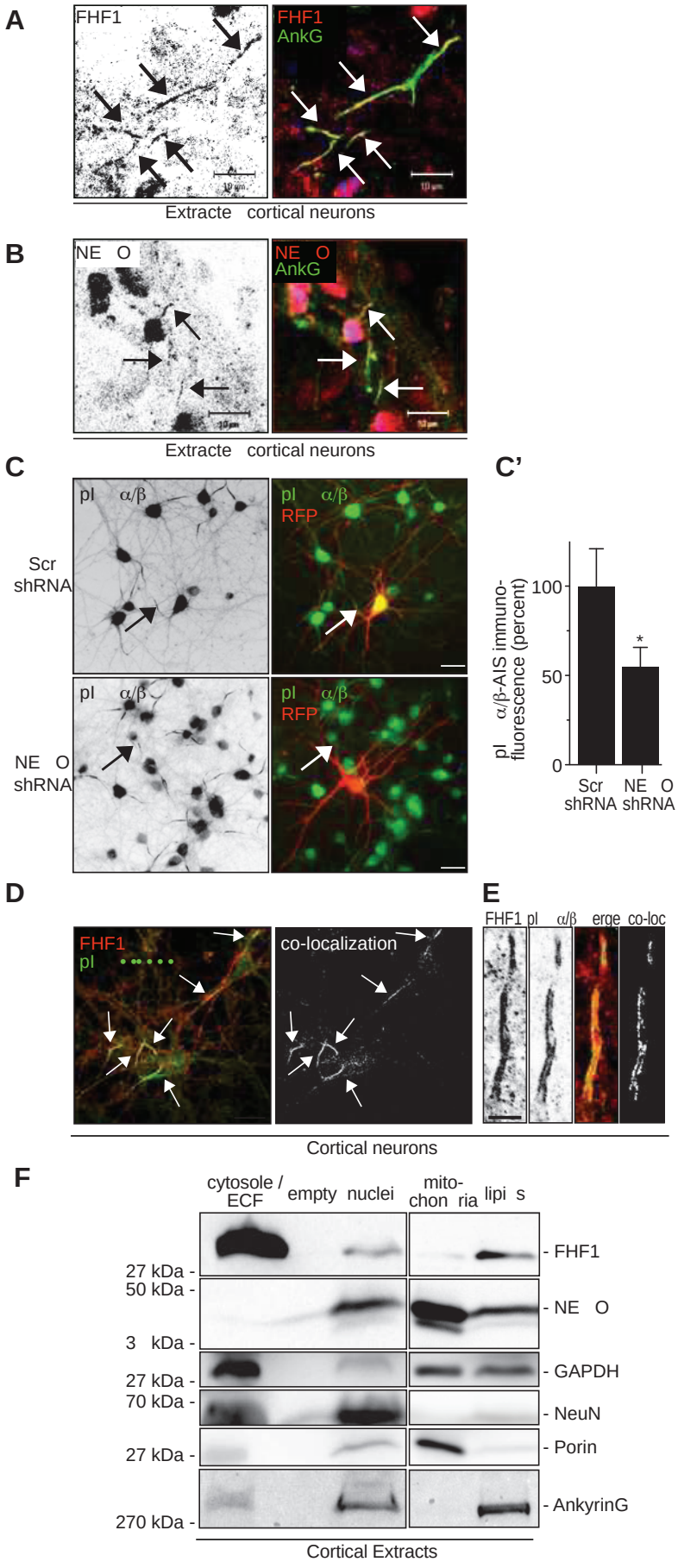
A
FHF1
FHF1
AnkG
Extracte cortical neurons
B
NE O
NE O
AnkG
Extracte cortical neurons
C
C'
pI α/β
pI α/β
RFP
Scr
shRNA
pI α/β
pI α/β
RFP
NE O
shRNA
pI α/β-AIS immuno-
fluorescence (percent)
100
50
0
*
Scr
shRNA
NE O
shRNA
D
E
FHF1
pI
co-localization
FHF1 pI α/β erge co-loc
Cortical neurons
F
cytosole /
ECF
empty
nuclei
mito-
chon
ria
lipi
s
27 kDa -
50 kDa -
3 kDa -
27 kDa -
70 kDa -
27 kDa -
270 kDa -
- FHF1
- NE O
- GAPDH
- NeuN
- Porin
- AnkyrinG
Cortical Extracts

Figure 4

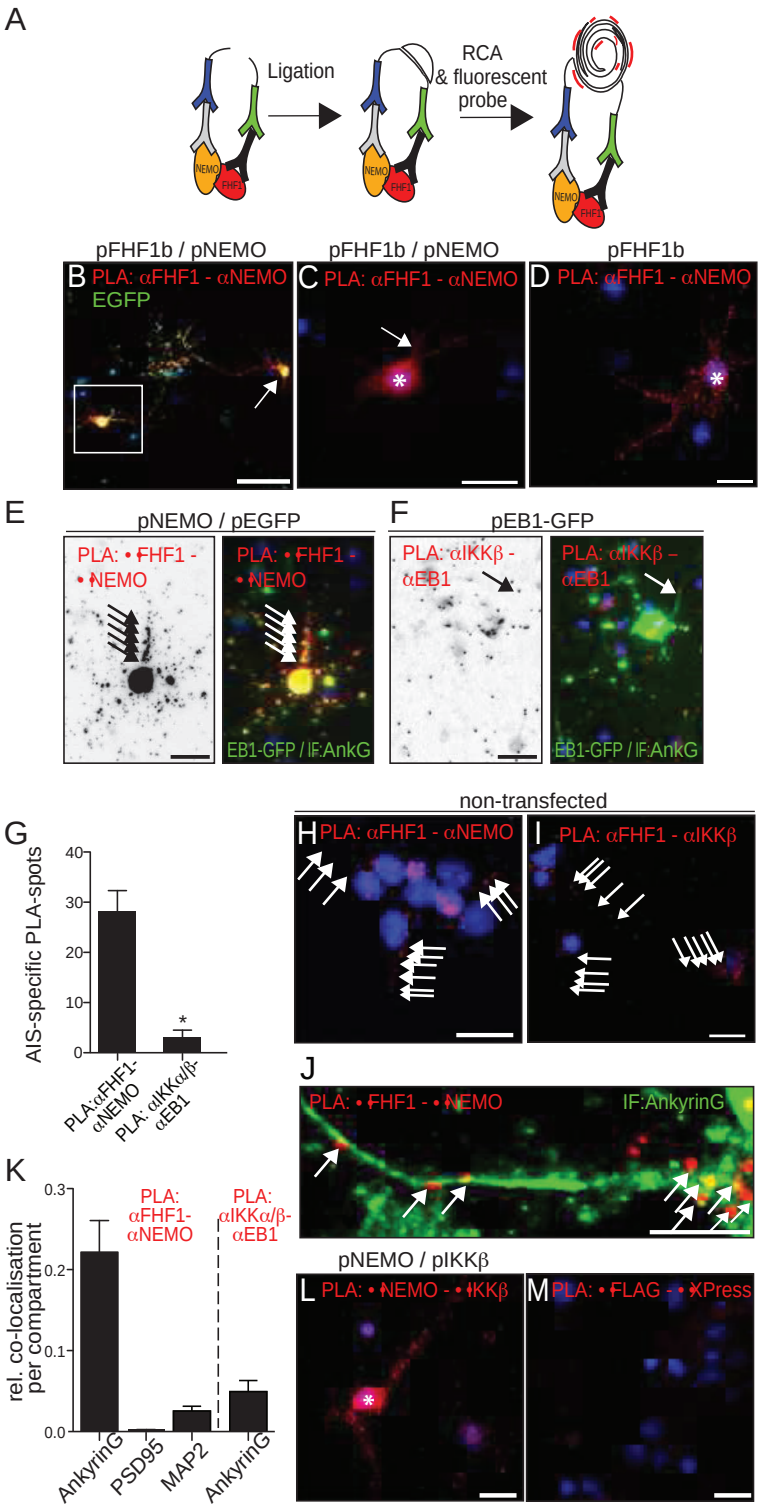
A
Ligation
RCA
& fluorescent
probe
NEMO
FHF1
pFHF1b / pNEMO
pFHF1b / pNEMO
pFHF1b
B PLA: αFHF1 - αNEMO
EGFP
C PLA: αFHF1 - αNEMO
D PLA: αFHF1 - αNEMO
E
pNEMO / pEGFP
PLA: • FHF1 -
• NEMO
PLA: • FHF1 -
• NEMO
EB1-GFP / IF:AnkG
F
pEB1-GFP
PLA: αIKKβ -
αEB1
PLA: αIKKβ –
αEB1
EB1-GFP / IF:AnkG
G
AIS-specific PLA-spots
40
30
20
10
0
*
PLA:αFHF1-
αNEMO
PLA: αIKKα/β-
αEB1
non-transfected
H PLA: αFHF1 - αNEMO
I PLA: αFHF1 - αIKKβ
J
PLA: • FHF1 - • NEMO
IF:AnkyrinG
K
rel. co-localisation
per compartment
0.3
0.2
0.1
0.0
PLA:
αFHF1-
αNEMO
PLA:
αIKKα/β-
αEB1
AnkyrinG
PSD95
MAP2
AnkyrinG
pNEMO / pIKKβ
L PLA: • NEMO - • IKKβ
M PLA: • FLAG - • XPress

Figure 5

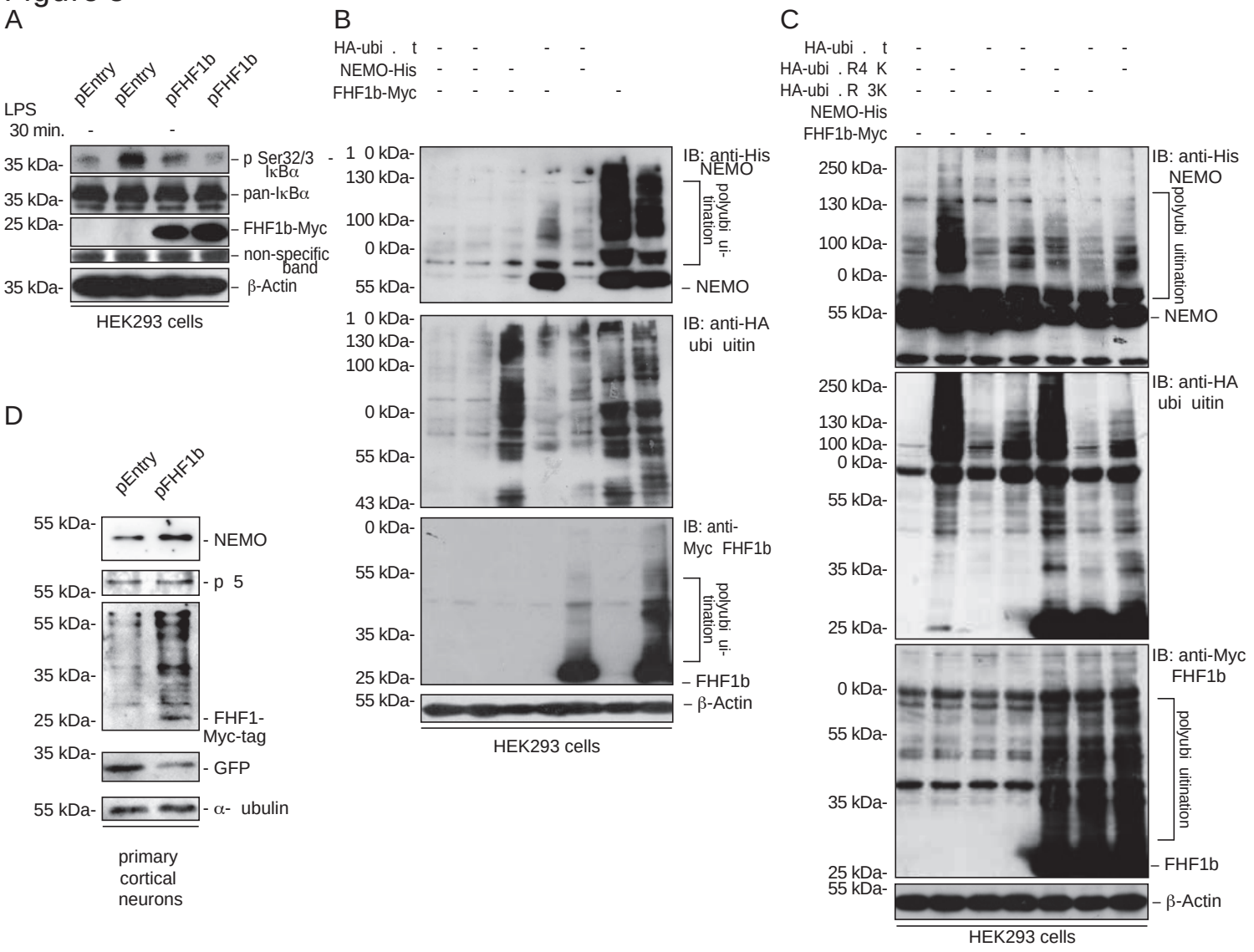
A
pEntry
pEntry
pFHF1b
pFHF1b
LPS
30 min.
35 kDa-
– p Ser32/3 - IκBα
35 kDa-
– pan-IκBα
25 kDa-
– FHF1b-Myc
– non-specific band
35 kDa-
– β-Actin
HEK293 cells
B
HA-ubi . t
NEMO-His
FHF1b-Myc
1 0 kDa-
130 kDa-
100 kDa-
0 kDa-
55 kDa-
IB: anti-His NEMO
polyubi ui- tination
– NEMO
IB: anti-HA ubi uitin
43 kDa-
IB: anti- Myc FHF1b
– FHF1b
– β-Actin
HEK293 cells
C
HA-ubi . t
HA-ubi . R4 K
HA-ubi . R 3K
NEMO-His
FHF1b-Myc
250 kDa-
130 kDa-
100 kDa-
0 kDa-
55 kDa-
IB: anti-His NEMO
polyubi uitination
– NEMO
IB: anti-HA ubi uitin
35 kDa-
25 kDa-
IB: anti-Myc FHF1b
– FHF1b
– β-Actin
HEK293 cells
D
pEntry
pFHF1b
55 kDa-
- NEMO
- p 5
- FHF1- Myc-tag
35 kDa-
- GFP
- α- ubulin
primary cortical neurons

F

A

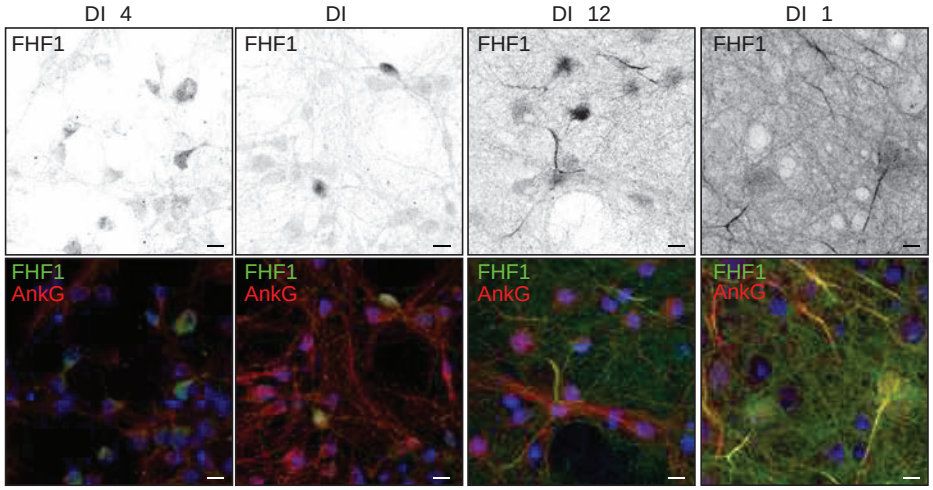
DI 4
DI
DI 12
DI 1
FHF1
FHF1
AnkG

B

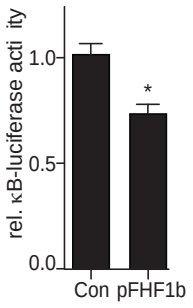
rel. κB-luciferase acti ity
1.0
0.5
0.0
*
Con
pFHF1b

C

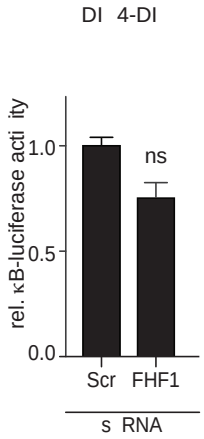
DI 4-DI
rel. κB-luciferase acti ity
1.0
0.5
0.0
ns
Scr
FHF1
s RNA

D

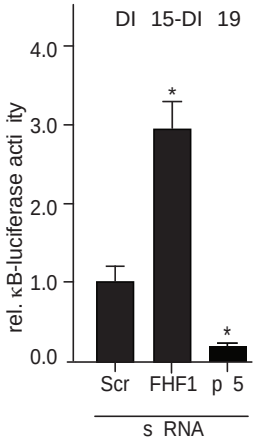
DI 15-DI 19
rel. κB-luciferase acti ity
4.0
3.0
2.0
1.0
0.0
*
Scr
FHF1
p 5
s RNA

E

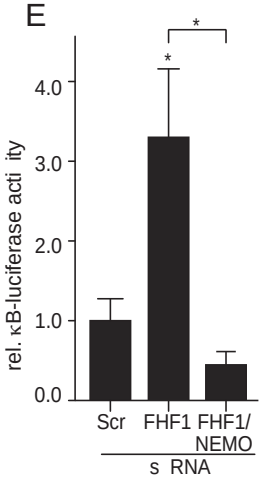
rel. κB-luciferase acti ity
4.0
3.0
2.0
1.0
0.0
*
*
Scr
FHF1
FHF1/
NEMO
s RNA

F

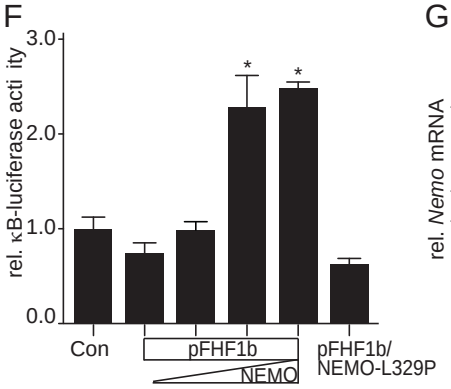
rel. κB-luciferase acti ity
3.0
2.0
1.0
0.0
*
*
Con
pFHF1b
NEMO
pFHF1b/
NEMO-L329P

G

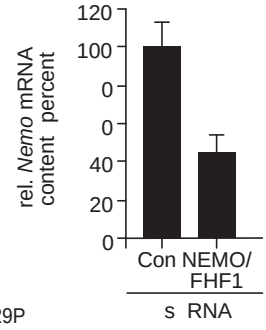
rel. Nemo mRNA
content percent
120
100
0
0
40
20
0
Con
NEMO/
FHF1
s RNA

H

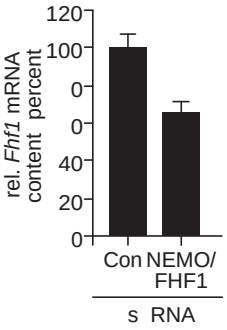
rel. Fhf1 mRNA
content percent
120
100
0
0
40
20
0
Con
NEMO/
FHF1
s RNA

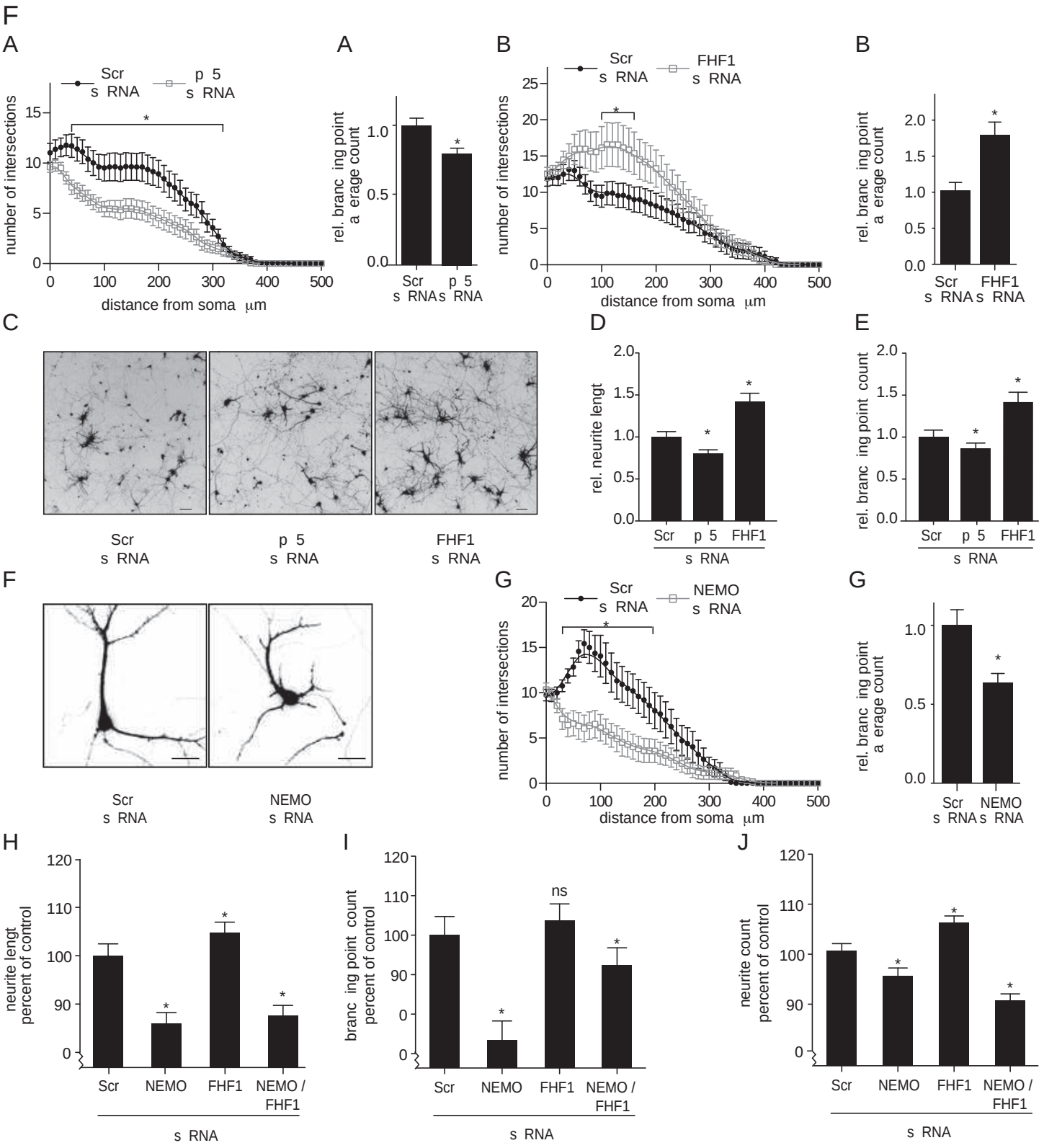
F
A
Scr
s RNA
p 5
s RNA
number of intersections
distance from soma μm
A
rel. branc ing point
a erage count
Scr
s RNA
p 5
s RNA
B
Scr
s RNA
FHF1
s RNA
number of intersections
distance from soma μm
B
rel. branc ing point
a erage count
Scr
s RNA
FHF1
s RNA
C
Scr
s RNA
p 5
s RNA
FHF1
s RNA
D
rel. neurite lengt
Scr
p 5
FHF1
s RNA
E
rel. branc ing point count
Scr
p 5
FHF1
s RNA
F
Scr
s RNA
NEMO
s RNA
G
Scr
s RNA
NEMO
s RNA
number of intersections
distance from soma μm
G
rel. branc ing point
a erage count
Scr
s RNA
NEMO
s RNA
H
neurite lengt
percent of control
Scr
NEMO
FHF1
NEMO /
FHF1
s RNA
I
branc ing point count
percent of control
ns
Scr
NEMO
FHF1
NEMO /
FHF1
s RNA
J
neurite count
percent of control
Scr
NEMO
FHF1
NEMO /
FHF1
s RNA

F

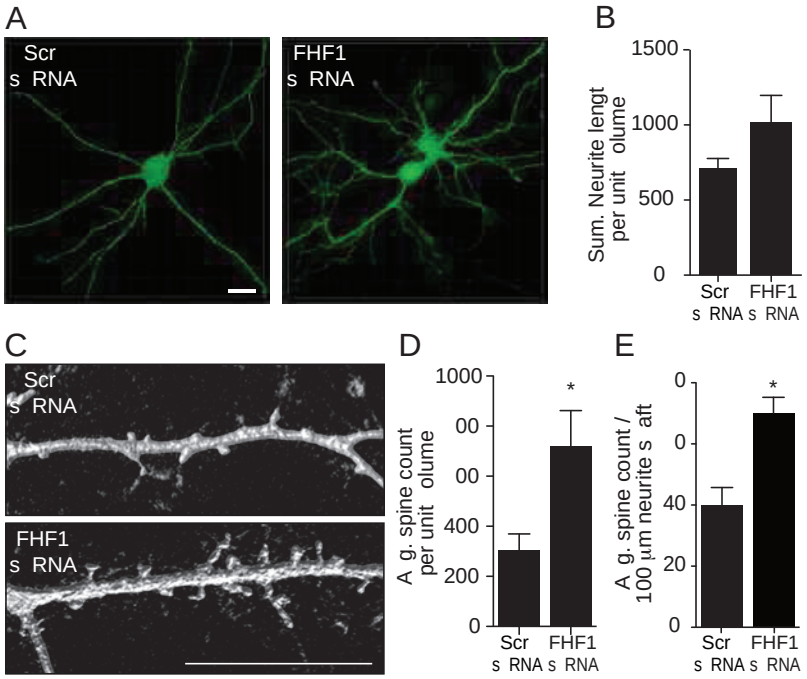
A
Scr
s RNA
FHF1
s RNA
B
1500
1000
500
0
Sum. Neurite lengt
per unit olume
Scr
s RNA
FHF1
s RNA
C
Scr
s RNA
FHF1
s RNA
D
1000
00
00
400
200
0
A g. spine count
per unit olume
*
Scr
s RNA
FHF1
s RNA
E
0
0
40
20
0
A g. spine count /
100 µm neurite s aft
*
Scr
s RNA
FHF1
s RNA

Supplementary Figure 1

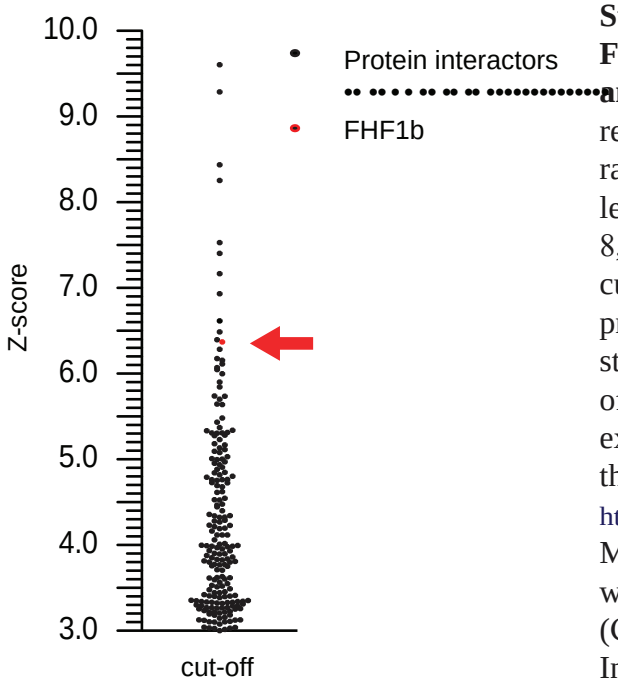

Supplementary Figure 1. The interaction between FHF1b and NEMO on Invitrogen Protoarrays ranges among the strongest hits. Biotinylated full-length human re-combinant NEMO was used to probe protein microar rays (Invitrogen Protoarray® version 4.0, Invitrogen, Pais-ley, UK). These arrays contained spots of approximately 8,200 full-length proteins. Hits were defined at a Z-score cut-off level of 3.0. Judged by this criterion a total of 112 protein interactors were identified. FHF1 was the twelfth strongest interactor with a Z-score of 6.37, within the range of the canonical NEMO interactors IKKα and IKKβ, which exhibited Z-scores of 5.70 and 8.25, respectively. A list of the interacting proteins can be found at the following link: http://www.ncbi.nlm.nih.gov/geo/query/acc.cgi?acc=GSE19841+ Microarray imaging and analysis were performed with a Perkin Elmer ScanArray Xpress 4 HT scanner (Cambridge, UK) and Z-scores were calculated using Invitrogen Protoarray Prospector version 5.1 software.

Supplementary Figure 2

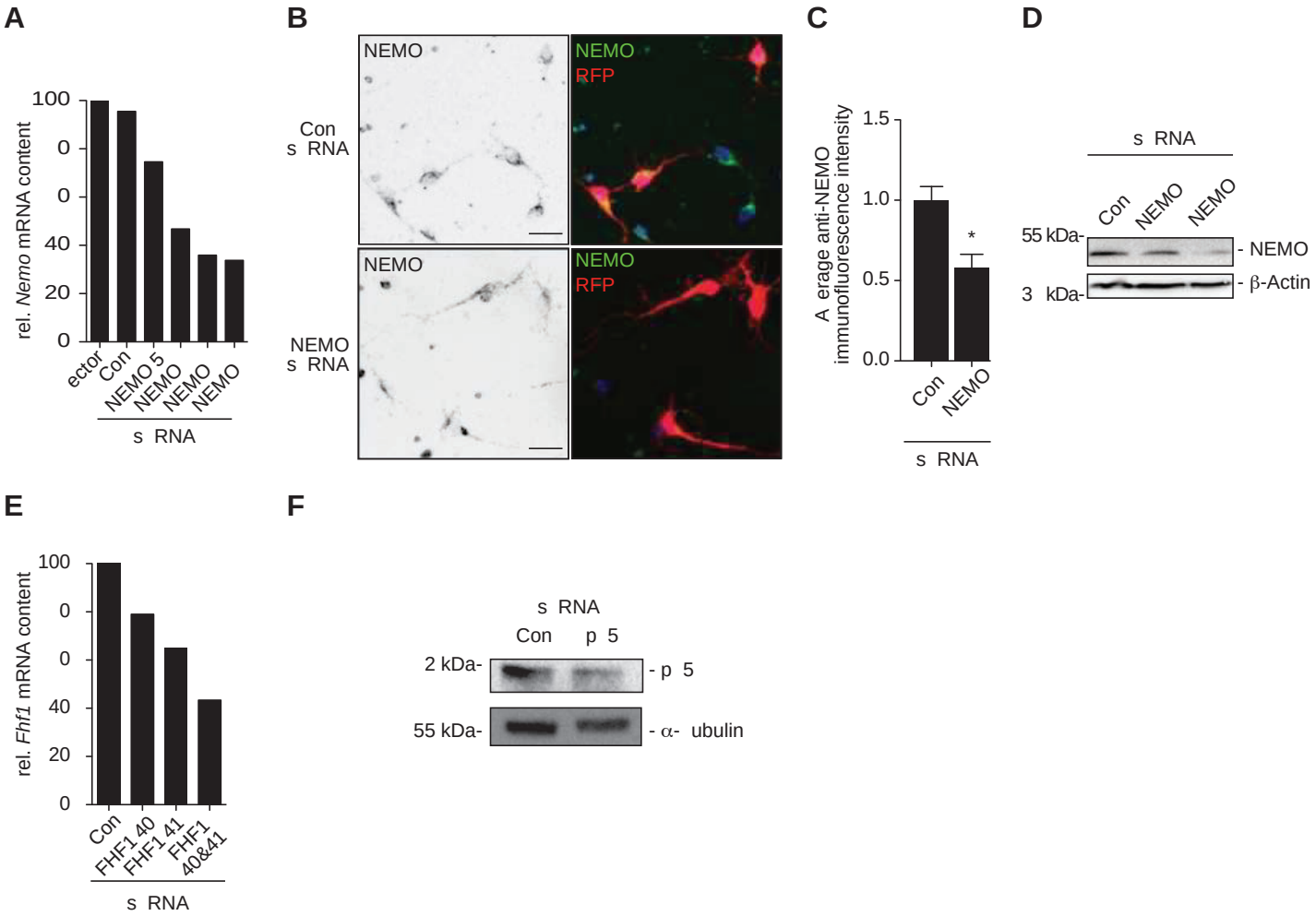

Supplementary Figure 2. Efficiency of RNA-silencing. (**A**) The relative *Nemo* mRNA content of rat phaechromocytoma cells (PC12) was determined using quantitative PCR three days after their transfection with small-hairpin vector constructs directed against different sections of the *Ikbkg/Nemo*-mRNA (Origene, Rockville, USA, FI7549-'05-08' in pRFP-C-RS) sequence as indicated. Values were normalized to *18S*-rRNA expression. (**B, C**) Freshly-dissociated cortical neurons were nucleofected with pools of two small-hairpin RNA vector constructs, directed to suppress NEMO expression, or control vector and plated. Three days following transfection, the cells were paraformaldehyde-fixed and examined by immunofluorescence analysis using a monoclonal mouse anti-NEMO antibody (NEMO, Abcam, green). Determination of total anti-NEMO immunofluorescence intensities in RFP-positive cells was determined from photomicrographs sampled from three wells (B, n = 34-39 cells, p = 0.0001, Mann-Whitney U test). (**D**) The NEMO protein content in PC12 cells was determined by Western-blotting experiments. Following three days of transfection with the above mentioned NEMO'7' and NEMO '8' labelled *Ikbkg/Nemo*-mRNA silencing constructs cells were lysed and the lysates subjected to Western-blot analyses, as indicated. Membranes were exposed to anti-NEMO antibodies (1:1000, Abcam) or β-actin (1:2000, Abcam) (**E**) Mature neuron cultures were transfected for four days with small-hairpin constructs directed against different sections of the rat *Fhf1*-mRNA sequence (pRS-shRNA FHF1'TR5104-40/41' (Origene) or a combination thereof. Their relative *Fhf1*-mRNA content was determined by normalization to *18S*-rRNA expression. Pooled introduction of two-shRNA sequences revealed their cumulative potency. (**F**) The p65 protein content in PC12 cells was determined by Western-blotting experiments. Following three days of transfection using the two most effective shRNA constructs targeting *RelA/p65* mRNA (Origene), cells were lysed and the lysates subjected to Western-blot analyses, as indicated. Membranes were exposed to anti-p65 (NLS) antibodies (1:500, Millipore) or α-Tubulin (1:5000, Sigma)

Supplementary Figure 3

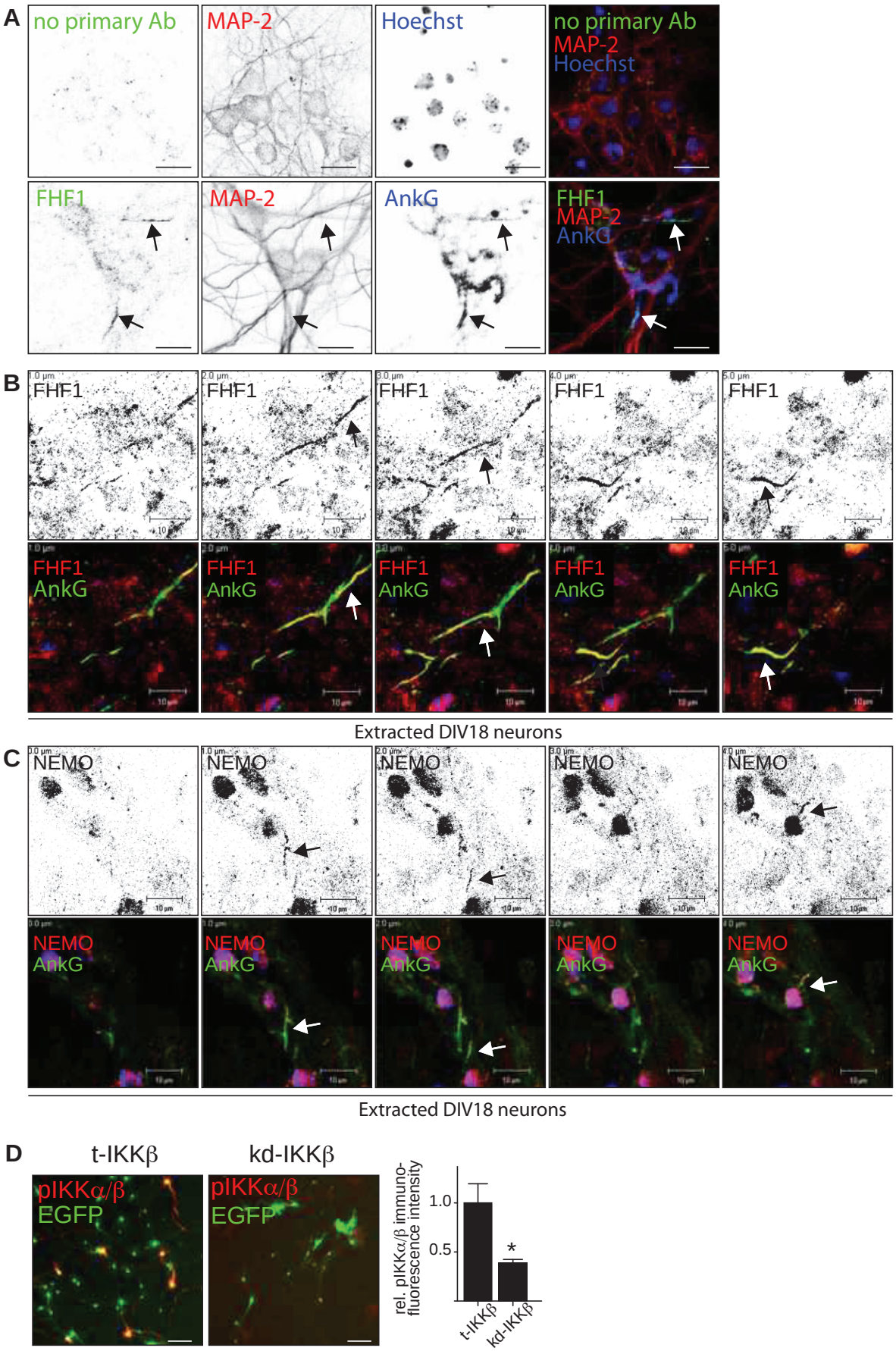

Supplementary Figure 3. Confirmation of specificity for anti-FHF1, anti-NEMO and anti-phosphorylated IKKβ immunofluorescence reactions. (**A**) Mouse cortical cultures were maintained for three weeks, half of the media was refreshed every four days. Following fixation using fresh 3 % paraformaldehyde solution for 12 minutes at 37°C, permeabilization and blocking, cells were either exposed to anti-mouse-FHF1 antibody in antibody solution (1:100, Abcam, overnight) or antibody solution only, as indicated.

Supplementary Figure 4

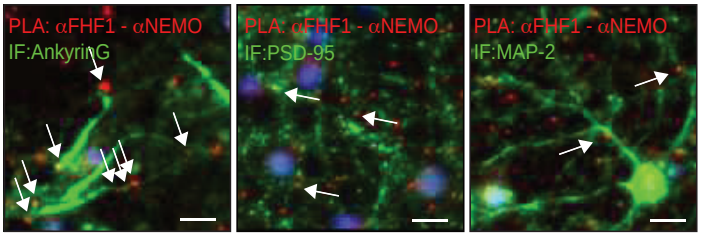

E tracted cortical neurons

Supplementary Figure 4: Endogenous NEMO / FHF1-interactions occur preferentially within the axon initial segment cytoskeleton. Proximity-ligation mediated between endogenous epitopes of FHF1 and NEMO. Prior to fixation, neurons were detergent extracted as described above, fixed and exposed to mouse anti-FHF1 and rabbit anti-NEMO antibodies. The PLA assay was conducted according to manufacturer's instructions. Red spots indicate amplification of fluorescently labeled oligonucleotides at locations of molecular proximity between epitopes. Subsequent to PLA assays, neurons were exposed to either mouse anti-AnkyrinG antibodies (Santa Cruz), anti-PSD-95 (Santa Cruz) or anti-MAP-2 (Santa Cruz) antibodies (green). The quantification of fluorescent spots co-localizing to the different neuronal compartments of the cell is depicted in Figure 4 (K). Scale bars, 10 μm.

Supplementary Figure 5

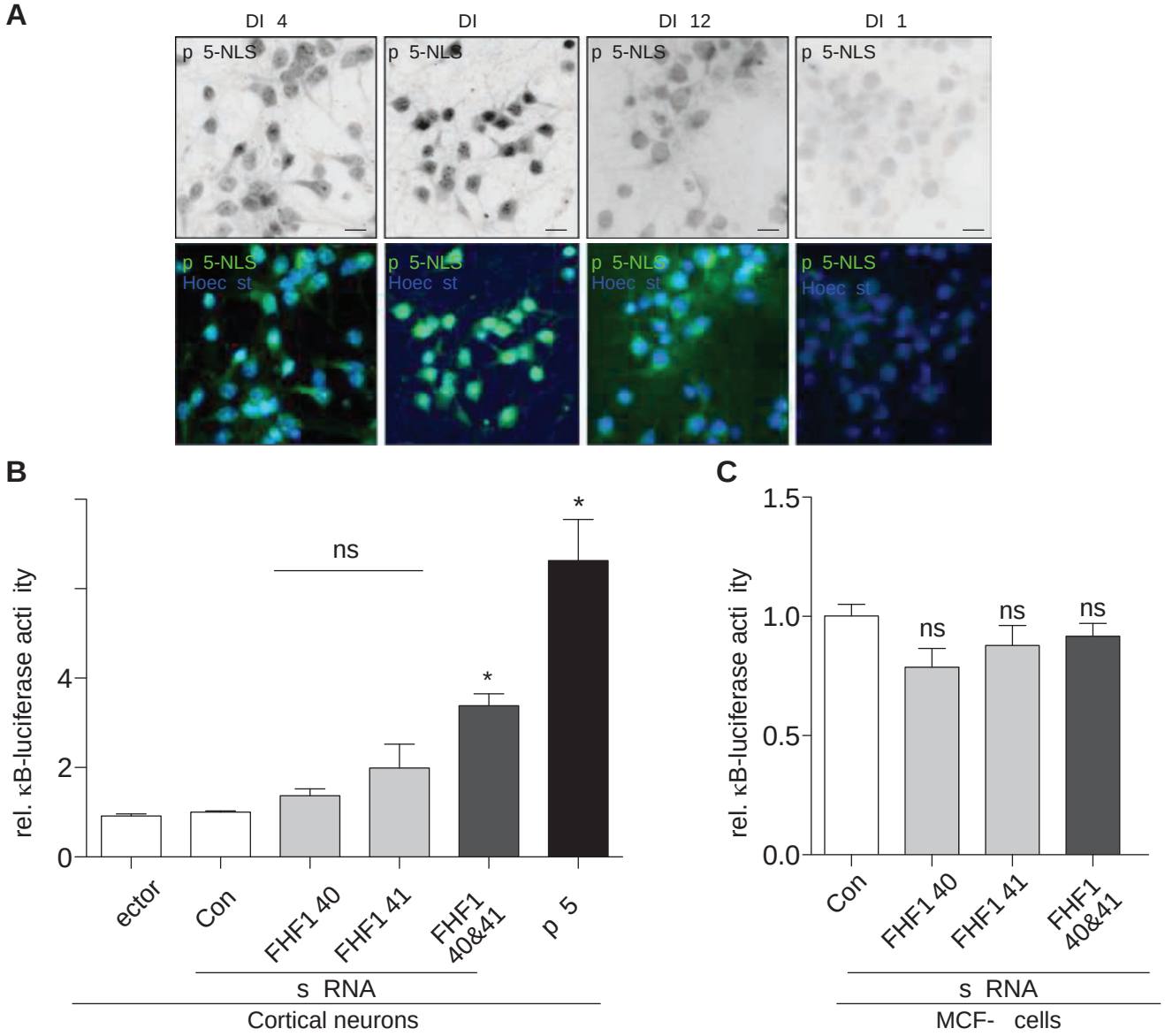

Supplementary Figure 5: Profile of active p65/NF-κB during *in vitro* development and evidence that the activation of NF-κB following *Fhf1*-silencing is sequence specific. (**A**) Mouse cortical neurons from one primary neuron preparation were cultured in parallel wells on poly-L-lysine coated cover-slips and removed at the indicated times points during *in vitro* development for direct fixation in -20°C methanole for two minutes. Standard immunofluorescence procedures were conducted using an antibody, raised against the solvent exposed nuclear localization sequence (NLS, anti-p65, 1:500, Millipore) of activated p65/NF-κB (green). Nuclei are depicted in blue. Note the pronounced increase in active transcription factor in the nucleus around DIV7. Scale bar, 20 µm. (**B**) Mature rat cortical neurons were transfected via calcium-phosphate DNA-precipitation between DIV14 - 18 using the small-hairpin RNA-interference vectors specific for *Fgf12/Fhf1* mRNA or wt-p65/NF-κB plasmid as indicated, and co-transfected with the κB dependent Firefly-luciferase and a constitutive thymidine kinase promoter driven Renilla-luciferase. After five days in culture, cells were lysed in passive lysis buffer and the relative κB-luciferase activity was determined using the Dual-Luciferase kit® (Promega, Madison, USA; n = 6 - 13 wells, from 3 pooled experiments. *,$p \leq 0.05$, one-way ANOVA followed by Dunn's multiple comparisons). (**C**) Human MCF-7 (breast adenocarcinoma) cells were cultured using standard techniques and transfected using Lipofectamine 2000® (Invitrogen), according to manufacturer's protocols as indicated and homologous to the transfections of neurons in (B). The human *Fgf12/FHF1*-sequence however contains nucleotide disparities compared to the mouse/rat sequence the small-hairpin vectors were designed against. No significant increase in κB-dependent luciferase activity could be observed (n = 4 - 13, ns, $p > 0.05$, one-way ANOVA followed by Dunn's multiple comparisons).

Immunolabelling was additionally performed using rabbit anti-MAP2 antibodies (SCBT, red) and anti-AnkyrinG antibodies (SCBT, blue). Follwing washing steps, secondary anti-mouse/rabbit/goat Alexa-488 (green)/568 (red)/647 (here depicted in blue, all 1:500, Invitrogen)-linked antibodies were incubated for one hour with the cells, and confocal image analyses were performed following washing and mounting procedures. Note the weak background residual fluorescence that is visible in the "no primary antibody" labelled photomicrograph from anti-mouse-Alexa488 only exposed cultures. Only very weak somatic and no AIS-labelling was detectable in this negative control. In contrast a clear AIS immunofluorescence is visible in mouse anti-FHF1 antibody exposed cultures (arrows). (**B,C**) Mouse cortical cultures were maintained for three weeks. Cytosolic extractions on the live cells were performed directly prior to fixation in 3 % paraformaldehyde solution. To this aim, the warm media was removed and cells were directly exposed to the ice-cold solution containing 1 % Triton X-100 in a microtubule destabilizing buffer for three minutes. Cells were immediately fixed at 37°C for 12 minutes and subjected to the standard immunofluorescence labelling procedures, antibody exposures were performed overnight using mouse anti-FHF1 (1:100, Abcam) or anti-NEMO (1:200, Abcam) together with rabbit anti-AnkyrinG (1:500, SCBT) and the appropriate set of secondary antibodies. Confocal stack analysis small pinhole settings provided z-slices at 1 µm distances, as labelled, with each slices depicted next to his neighbour. Single images from this stack are depicted in Figure 3A and B. Note the close co-localization of FHF1 (red, B), as well as NEMO (red, C), to several AnkyrinG (green) positive AIS's throughout the different levels of the confocal stack analysis. (**D**) Adult cortical neurons were transfected using 1.5 µg either wild-type IKKβ or K44M-IKKβ (kd, kinase-dead, Addgene plasmids 11103&11104) together with EGFP-N1 vector (1.5 µg) to mark positively-transfected cells for two days. Cells were fixed as described above and subjected to the standard immunofluorescence protocol, using antibodies raised against Ser176/180 // Ser177/181-IKKα//β (red, anti-pIKKα/β, 1:500, clone 16A6, Cell Signaling Technology). Note the marked increase in immunofluorescence intensities in wild-type IKKβ/EGFP co-transfected cells, but not in K44M-IKKβ/EGFP co-transfected cells (wild-type IKKβ versus K44M-IKKβ, decreased by 0.61 ± 0.229, n = 17 cells, p = 0.0000001, Mann-Whitney U-test on the Log transformed data). EGFP co-transfection served to mark transfected cells . Scale bar, 10 µm in A-C, 50 µm in D.